Am J Cancer Res 2017;7(3):433-447
www.ajcr.us /ISSN:2156-6976/ajcr0050452

Original Article

Gpr110 deficiency decelerates carcinogen-induced hepatocarcinogenesis via activation of the IL-6/STAT3 pathway

Benting Ma[1,2*], Junjie Zhu[4*], Juan Tan[1], Yulei Mao[1], Lingyun Tang[1], Chunling Shen[1], Hongxing Zhang[1], Ying Kuang[3], Jian Fei[3], Xiao Yang[2], Zhugang Wang[1,2,3]

[1]State Key Laboratory of Medical Genomics, Research Center for Experimental Medicine, Rui-Jin Hospital Affiliated to Shanghai Jiao Tong University School of Medicine (SJTUSM), Shanghai 200025, China; [2]Department of Medical Genetics, E-Institutes of Shanghai Universities, SJTUSM, Shanghai 200025, China; [3]Shanghai Research Center for Model Organisms, Shanghai 201203, China; [4]Thoracic Surgery Laboratory, Shanghai Pulmonary Hospital Affiliated to Tong Ji University School of Medicine, Shanghai 200433, China. [*]Equal contributors.

Received February 9, 2017; Accepted February 17, 2017; Epub March 1, 2017; Published March 15, 2017

Abstract: Hepatocarcinogenesis is a complex process that includes pronounced necroinflammation, unregulated hepatocyte damage, subsequent extensive fibrosis, and carcinogenesis. *GPR110* was an adhesion G protein-coupled receptor. Analysis of the expression pattern of *Gpr110* in mice displayed that *Gpr110* was expressed highly in liver, implicating the tissue compartments where Gpr110 could execute its functions, the role of Gpr110 in the physiological and pathological state of liver remains unclear. Based on a *Gpr110* knockout mouse model, we evaluated the role of *Gpr110* in hepatocarcinogenesis by using a carbon tetrachloride (CCl_4)-induced liver injury and fibrosis model, as well as diethylnitrosamine (DEN) plus CCl_4-induced liver cancer model. In this study, we found subdued chronic liver injury, reduced compensatory proliferation, lower liver fibrosis, but enhanced inflammation occurred in *Gpr110*$^{-/-}$ mice during CCl_4 challenge. In addition, *Gpr110*$^{-/-}$ mice were resistant to liver tumorigenesis induced by DEN plus CCl_4 injection. Molecular mechanisms underlying these differences correlated with augmented activation of the IL-6/STAT3 pathway, which exerted hepatoprotective effects during liver damage, fibrosis, and oncogenesis in *Gpr110*$^{-/-}$ mice. Furthermore, pharmacological inhibition of the activation of the IL-6/STAT3 pathway enhanced hepatic fibrosis and promoted DEN plus CCl_4-induced carcinogenesis in *Gpr110*$^{-/-}$ mice. In summary, absence of *Gpr110* decelerates liver fibrosis/cirrhosis progressing into tumorigenesis, due to strengthening activation of the IL-6/STAT3 pathway, leading to a weaker liver injury and fibrosis microenvironment. It is indicated that targeting Gpr110 and activating the IL-6/STAT3 pathway may be considered to be preventive methods for some cirrhosis transition.

Keywords: Gpr110, CCl_4, hepatocarcinogenesis, knockout mouse model, fibrosis

Introduction

Hepatocellular carcinoma (HCC) is the typical of chronic tissue injury-associated cancer [1]. Chronic liver injury, which triggers perpetual hepatocellular damage, hepatocyte regeneration, and inflammation, is thought to be the established background that promotes neoplasia in these pathophysiologically distinct diseases [2]. HCC has clearly defined etiological factors, including viral hepatitis, nonalcoholic steatohepatitis (NASH), alcoholic liver disease, andcirrhosis [3]. Cirrhosis, which develops from long-term chronic liver disease, is considered to be the primary risk factor leading to HCC [4]. However, the molecular mechanisms responsible for this malignant transformation are still not understood.

Adhesion GPCRs, which have more than 60 receptors in vertebrate genomes, including 31 members in mice and 33 members in humans [5], are characterized by extremely long N-terminal regions and a GPCR-like seven-pass transmembrane domain [6, 7]. In recent years, since aberrant expressions of several adhesion-GPCR molecules have been identified in various human cancers, they have been

closely associated with cancer development. Forexample, BAI1 was downregulated in glioblastomas [8, 9], colorectal cancer [10] and gastric cancers [11]; GPR124 was identified as a tumor endothelial marker [12], promoting tumor angiogenesis; GPR56 was reported to be highly expressed in human gliomas [13]. With the gradual identification of adhesion GPCRs in various tumors, it is advisable to pay more attention to study the role of these interesting molecules in tumorigenesis and to explore more possibilities for their use in drugs [14].

GPR110, an orphan receptor that is highly conserved among species, belongs to members of the adhesion G protein-coupled receptor family. To date, its physiological function remains unknown. Lum et al. identified *GPR110* as a potential oncogene in murine T cell lymphomas during a large-scale retroviral insertion mutagenesis screening [15]. Subsequently, they detected overexpression of the GPR110 transcript and protein in the majority of lung (74%) and prostate (59%) adenocarcinomas, as well as related cell lines. Therefore, it can be assumed that GPR110 may participate in tumor development. However, the relationship between Gpr110 and hepatocarcinogenesis in vivo is as yet unknown.

Here we used *Gpr110* knockout mice to study the role of Gpr110 in hepatocarcinogenesis. We found that deficiency of *Gpr110* impeded DEN plus CCl_4-induced HCC formation. Moreover, the absence of *Gpr110* alleviated CCl_4-mediated liver injury and hepaticfibrosis, and ultimately delayed the development of cirrhosis and progression into HCC. Mechanistically, disruption of *Gpr110* triggered increased activation of the IL-6/STAT3 pathway, which decelerated chronic liver injury-driven hepatocarcinogenesis.

Materials and methods

DEN plus CCl_4-induced liver cancer model

Mice with a homozygous deletion of *Gpr110* were maintained on a 129SvJ background (Supplementary Figure 2). The procedures described were approved by the Animal Care and Use Committee of Shanghai Jiao Tong University School of Medicine. The liver tumor model induced by DEN plus CCl_4 was generated according to the previous reports [16, 17]. Briefly, 15-day-old male *Gpr110*$^{-/-}$ mice and their male wild-type littermates were intraperitoneally injected with a single dose of DEN (25 mg/kg), and then with 5 ml/kg body weight of 10% CCl_4 (dissolved in olive oil) twice a week from the age of 4 weeks. The mice were sacrificed at 4, 5, and 6 months post-CCl_4, and liver tissues were excised for experiments.

CCl_4-induced liver injury

Four- to six-week-old male *Gpr110*$^{-/-}$ mice and their male wild-type littermates were intraperitoneally injected with a single dose of CCl_4 (4 ml/kg, 10% dissolved in olive oil). The mice were sacrificed at 0, 24, 48, and 72 hours post-CCl_4, and liver tissues were excised for experiments.

CCl_4-induced liver fibrosis

Four- to six-week-old male *Gpr110*$^{-/-}$ mice and their male wild-type littermates were intraperitoneally injected with CCl_4 (4 ml/kg, 10% dissolved in olive oil) three times a week [17, 18]. The mice were sacrificed at 0, 2, 4, and 8 weeks post-CCl_4, and liver tissues were excised for experiments.

Inhibitor treatment

Specific p-Stat3 inhibitor, Stattic (Selleck Chemicals, USA), was injected at 3.75 mg/kg every other day, i.p., for four weeks, or at 3.75 mg/kg twice a week for four months.

Histology of mouse liver tissues

Formalin-fixed liver samples were paraffin-embedded, and paraffin sections (5 μm) were stained with hematoxylin and eosin (H&E) for analysis of morphologic changes. Liver fibrosis was determined by Sirius red staining. Immunohistochemistry and Sirius red staining were performed according to routine protocol. The primary antibodies were as follows: anti-Gpr110 (sc-292423, Santa Cruz, CA, USA,1:50), anti-α-SMA (A5228, Sigma, CA, USA, 1:200), anti-F4/80 (ab6604, Abcam, MA, USA, 1:100), anti-AFP (A0200, Abclonal, MA, USA, 1:200), anti-Collagen1 (sc-59772, Santa Cruz, CA, USA, 1:50), and anti-Tgf-β (GTX110630, GeneTex, CA, USA, 100). Apoptosis was assessed by TUNEL staining of paraffin-embedded slides (11684795910, Roche, Mannheim, Germany).

Proliferation was assessed by immunostaining for BrdU (#MS-1058-B0, Thermo Fisher Scientific Inc. Rockford, CA, USA, 1:200) staining.

Blood chemistry

Mice were sacrificed at different time points after CCl_4 treatment. Blood was drawn via cardiac puncture into heparinized tubes and centrifuged (5,000 rpm, 15 min, 4°C). Plasma was collected and stored at -80°C for further analysis. Serum AST, ALT and other serum biochemical indicators were measured using a Fuji DRICHEM 55500 V (sysmex System, Tokyo, Japan) according to the manufacturer's instructions.

TUNNEL assay

Apoptotic cells on sections were detected using an In Situ Cell Death Detection Kit (Roche) according to the manufacturer's protocol. Images were taken with a Nikon fluorescent microscope.

BrdU staining

Cell proliferation in livers were measured by the incorporation of BrdU, which was administered i.p. to mice at a dosage of 50 μg/g body weight 2 h before killing. BrdU incorporation was detected on sections by immunohistochemistry.

Cell culture

The SMMC-7721 HCC cell line was obtained from the Shanghai Cell Bank (Shanghai, China). The Huh7 cell line was obtained from the American Type Culture Collection (Manassas, VA). Cells were routinely cultured in DMEM medium (Hyclone) supplemented with 10% fetal bovine serum (FBS, Gibco) within a humidified incubator containing 5% CO_2 at 37°C.

Western blotting

Whole mouse liver tissues were homogenized in Triton lysis buffer (20 mM Tris, pH 7.4, 137 mM NaCl, 10% glycerol, 1% Triton X+100, 2 mM EDTA, 1 mM PMSF, 10 mM NaF, 5 mg/ml aprotinin, 20 mM leupeptin, and 1 mM sodium orthovanadate) and centrifuged at 13,000 rpm at 4°C for 15 min. Protein extracts were separated by 8-16% SDS-PAGE and analyzed using the following primary antibodies: anti-CYP2E1 (A2160, Abclonal, MA, USA, 1:500), anti-a-SMA (A5228, Sigma, CA, USA, 1:200), anti-Collagen1 (sc-59772, Santa Cruz, CA, USA, 1:500), and anti-Tgf-β (GTX110630, GeneTex, CA, USA, 1000), anti-IL-6 (GTX31178, GeneTex, CA, USA, 1:500), anti-p-Stat3 (#9145, Cell Signaling Technology, MA, USA, 1:1000), anti-stat3 (#4904, Cell Signaling Technology, MA, USA, 1:1000), anti-p-ERK (#9101, Cell Signaling Technology, MA, USA, 1:1000), anti-p-P38 (#9211, Cell Signaling Technology, MA, USA, 1:1000), and anti-p50/105 (ADI-KAP-TF112, ENZO, NY, USA, 1:1000). Secondary antibodies were labeled with IRDye 700 (Rockland Immunochemicals). Protein levels were detected using the Odyssey system (LiCor, Lincoln, NE).

Cytokine measurement in serum

Mice were sacrificed at different time points after CCl_4 treatment. Blood was drawn via cardiac puncture into heparinized tubes and centrifuged (5,000 rpm, 15 min, 4°C). Serum was collected and stored at -80°C for further analysis. Levels of IL-6, IL-1β, TNF-α and MIP2 were detected with a commercial ELISA kit following the instructions of the manufacturer (Dakewei, Shenzhen, China) (Synergy H1Hybrid Reader, BioTek, USA).

Measurement of IL-6 in liver tissue homogenates

Mice were sacrificed at different time points after CCl_4 treatment. For the measurement of IL-6, equal weights of liver tissues (100 mg) from various groups were sonicated in 1 ml of phosphate buffer saline containing protease inhibitor cocktail. Homogenates were cleared by centrifuging at 10,000 rpm at 4°C for 15 min. The supernatants were transferred to another new tube, liver IL-6 levels were normalized to the total protein in the homogenates, which was detected with a commercial ELISA kit following the instructions of the manufacturer (Dakewei, Shenzhen, China) (Synergy H1Hybrid Reader, BioTek, USA).

Quantitative real-time PCR analysis

Total RNA was prepared from mouse liver tissues using Trizol Reagent (Invitrogen) according to the manufacturer's instructions. Real-time

PCR analysis was performed using a SYBR Premix Ex Taq kit (Takara, Dalian, China) on an Eppendorf Mastercycler system according to the manufacturer's instructions. The expression of specific transcript was normalized against β-actin, and the experiments were repeated in triplicate. The primers used are listed in Supplementary Table 1.

Statistical analysis

Data were presented as means ± SD, while quantitative variables were analyzed using *t*-test. All statistical tests were two-sided, and $P<0.05$ was regarded as statistically significant.

Results

Deletion of Gpr110 alleviated CCl_4-mediated acute hepatic injury and compensatory proliferation

To determine the expression pattern of *Gpr110* in mice, we performed semi-quantitative and real-time reverse transcription (RT)-PCR analyses on various mouse tissues. As shown in Supplementary Figure 1, the highest expression level of *Gpr110* mRNA was found in the prostate, and the second highest was found in the kidney and liver, implicating the tissue compartments where Gpr110 could execute its physiological functions in mice. To assess the biological functional role of Gpr110 in vivo, we generated a mouse model with global-targeted deletion of *Gpr110*. As expected, Gpr110 mRNA and proteins were disrupted in *Gpr110*$^{-/-}$ mice (Supplementary Figure 2). However, after a global-targeted deletion of *Gpr110* mice were born alive and appeared grossly normal (Supplementary Figure 3), suggesting that Gpr110 is not indispensable for normal development. Interestingly, pathological analysis showed a smaller necrosis area existed in *Gpr110*$^{-/-}$ mice compared with their wild-type littermates after CCl_4 challenge (**Figure 1A**, **1B**). Meanwhile, serum alanine transaminase (ALT) and aspartate transaminase (AST) levels were significantly lower in *Gpr110*$^{-/-}$ mice compared to control mice, resulting in subdued hepatocellular damage in *Gpr110*$^{-/-}$ mice (**Figure 1C**, **1D**). In addition, TUNEL assay results revealed that the number of apoptotic hepatocytes was significantly lower in *Gpr110*$^{-/-}$ mice than in wild-type mice post CCl_4 injection (**Figure 1E**, **1F**). As we have known, p450 CYP2E1-mediated CCl_4 metabolism is required for CCl_4-induced liver injury [19]. Therefore, we examined whether the reduction of liver injury in *Gpr110*$^{-/-}$ mice was due to alterations of CCl_4 metabolism. As shown in Supplementary Figure 4, Expression of CYP2E1 was similar in liver tissues from control and *Gpr110*$^{-/-}$ mice, suggesting no difference between the two groups on CCl_4 metabolism. Owing to the high regenerative capacity of the liver, even when some fractions of hepatocytes undergo cell death in response to CCl_4, the remaining surviving hepatocytes should undergo a compensatory proliferative response. BrdU-labeling of proliferating cells showed that the number of compensatory proliferating hepatocytes was significantly lower in *Gpr110*$^{-/-}$ mice than in wild-type mice after CCl_4 challenge (**Figure 1G**, **1H**), which indicated that deletion of *Gpr110* further impeded hepatic compensatory proliferation after CCl_4 treatment. Usually, acute liver diseases are accompanied by inflammation, and inflammation is considered to be an important factor in hepatocellular damage [20, 21]. However, we found that *Gpr110*$^{-/-}$ mice were more susceptible to CCl_4-induced liver acute inflammation by detecting of several hepatic inflammatory cytokines and inflammatory cell markers (Supplementary Figure 5). Moreover, clinical data have also shown that inflammation does not always kill hepatocytes during liver damage in some patients [22, 23]. In conclusion, these results suggest that inflammation may do not correlate with hepatocellular injury induced by CCl_4. Taken together, these observations demonstrate that deficiency of *Gpr110* weakened hepatocellular damage, but enhanced inflammation induced by CCl_4.

Gpr110$^{-/-}$ *mice displayed a lower level of hepatic fibrosis compared with wild-type mice after CCl_4 administration*

To assess whether deletion of *Gpr110* also mitigated liver fibrosis, a model of long-term CCl_4 administration was used. After two, four, and eight weeks of CCl_4 treatment, fibrotic changes were also noticeable, *Gpr110*$^{-/-}$ mice displayed subdued hepatic fibrosis (**Figure 2A**, **2B**). Western blot and immunohistochemical analysis also confirmed that lower expressions of liver fibrosis-related molecular Collagen-1 and TGF-β in the liver were found in *Gpr110*$^{-/-}$ mice compared to their wild-type littermates (**Figure 2C-F**, **2I**). Given that hepatic stellate cells

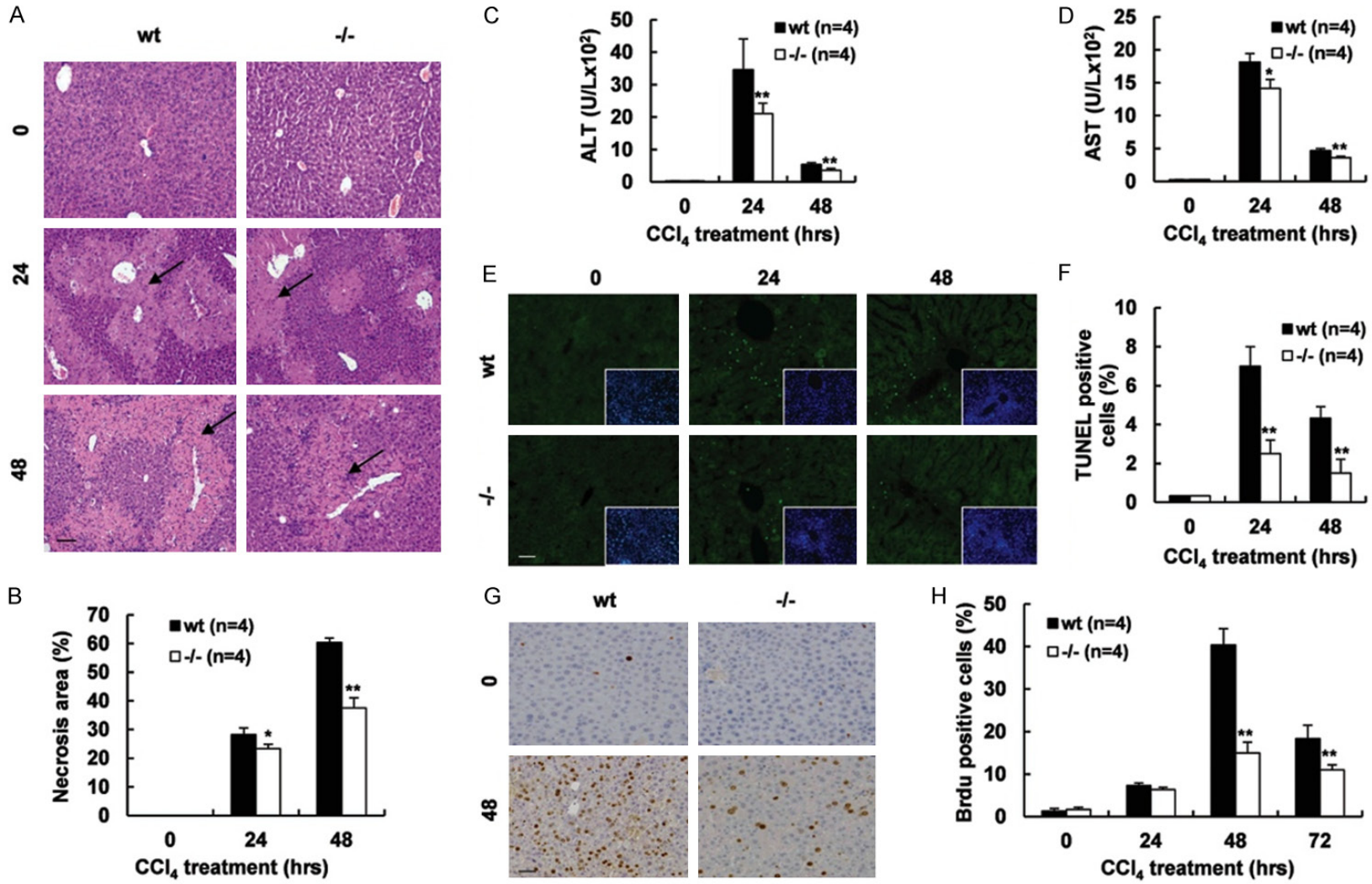

Figure 1. Disruption of *Gpr110* weakened CCl_4-induced hepatic acute injury and hepatocyte compensatory proliferation. (A, B) H&E staining of sacrificed *Gpr110*$^{-/-}$ mice and wild-type littermate liver sections (100×), mice were treated CCl_4 for 0-, 24- and 48 hours (A). Scalebar, 100 μm. Percentage of necrosis area were quantified with the ImageJ software and statistical analyzed (B). Values are presented as mean ± SD. **P*<0.05; **P<0.01. (C, D) Serum ALT, AST levels were determined at 0, 24 and 48 hours after the CCl_4 injection (n=4) and statistical analyzed. Values are presented as mean ± SD. **P*<0.05; **P<0.01. (E, F) TUNEL staining of liver sections from 0-, 24- and 48 hours after the CCl_4 injection-sacrificed *Gpr110*$^{-/-}$ mice and wild-type littermate mice liver (200×) (E). Scalebar, 50 μm. Quantified by statistical analyzing percentage of positive cells in 20 high-power fields (F). Values are presented as mean ± SD. **P*<0.05; **P<0.01. (G, H) Representative immunohistochemical staining of BrdU, sections from 0- and 48 hours after the CCl_4 injection-sacrificed *Gpr110*$^{-/-}$ mice and wild-type littermate mice liver (200×) (G). Scalebar, 50 μm. Quantified by statistical analyzing percentage of positive cells in 20 high-power fields (H). Values are presented as mean ± SD. **P*<0.05; **P<0.01.

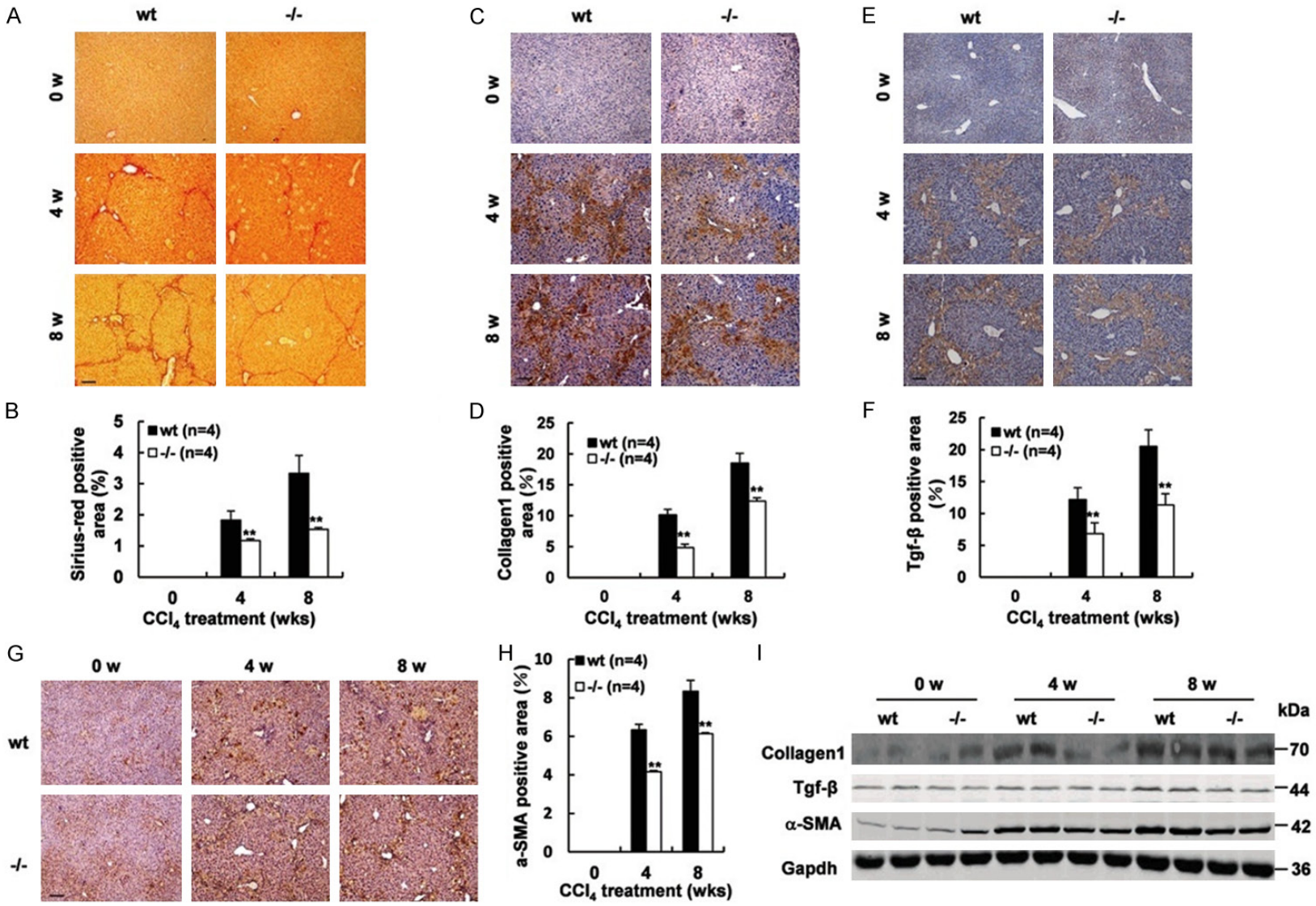

Figure 2. Deletion of *Gpr110* caused less evident liver fibrosis and HSC activation upon chronic CCl_4 challenges. (A, B) Mice were treated with CCl_4 for 0, 4 and 8 weeks (n=6). Siriusred staining sections from 0-, 4- and 8 weeks after the CCl_4 injection-sacrificed *Gpr110*$^{-/-}$ mice and wild-type littermate mice liver (100×) (A). Scalebar, 100 μm. Percentage of Sirius red positive area were quantified with the ImageJ software and statistical analyzed (B). Values are presented as mean ± SD. **P*<0.05; **P<0.01. (C, D) Immunostaining of Collagen1, sections from 0-, 4- and 8 weeks after the CCl_4 injection -sacrificed *Gpr110*$^{-/-}$ mice and wild-type littermate

mice liver (100×) (C). Scalebar, 100 μm. Percentage of collagen1 positive area were quantified with the ImageJ software and statistical analyzed (D). Values are presented as mean ± SD. *P<0.05; **P<0.01. (E, F) Immunostaining of Tgf-β, sections from 0-, 4- and 8 weeks after the CCl_4 injection-sacrificed *Gpr110*$^{-/-}$ mice and wild-type littermate mice liver (100×) (E). Scalebar, 100 μm. Percentage of Tgf-β positive area were quantified with the ImageJ software and statistical analyzed (F). Values are presented as mean ± SD. *P<0.05; **P<0.01. (G, H) Immunostaining of α-SMA, sections from 0-, 4- and 8 weeks after the CCl_4 injection-sacrificed mice liver (100×) (G). Scalebar, 100 μm. Percentage of Tgf-β positive area were quantified with the ImageJ software and statistical analyzed (H). Values are presented as mean ± SD. *P<0.05; **P<0.01. (I) Western blot analysis of Collagen1, Tgf-β and α-SMA in 0-week, 4-week and 8-week CCl_4-treated *Gpr110*$^{-/-}$ mice and wild-type littermate mice liver.

(HSCs) have a critical role in inducing fibrosis, and that the α-smooth muscle actin (α-SMA) was considered as the marker of activated HSCs, we detected the expression levels of α-SMA. As shown in **Figure 2F-I**, decreased α-SMA was found in the *Gpr110*$^{-/-}$ group after CCl_4 treatment. Since chronic inflammation is known to play an important role in fibrosis, we assessed inflammatory markers and infiltrate. As shown in Supplementary Figure 6, the difference did not appear to be significant. Thus, these results demonstrated the importance of Gpr110 in CCl_4-mediated chronic liver fibrosis. Collectively, these data suggest that deletion of *Gpr110* abated CCl_4-mediated hepatocyte injury, which possibly led to subsequent fibrotic changes and tumor formation.

Absence of Gpr110 restrained carcinogen-induced hepatocarcinogenesis, weakened fibrosis, and prolonged survival time

It has been well established that most patients with HCC developed as a result of chronic injury, fibrosis, and hepatocarcinogenesis. Meanwhile, using the Cancer Genome Atlas (TCGA) database, we found the gene copy number of GPR110 in hepatocellular carcinoma was significantly different from the level in normal samples (Supplementary Figure 7). To elucidate whether Gpr110 regulated hepatocarcinogenesis in vivo, we used 15-day-old *Gpr110*$^{-/-}$ mice. *Gpr110*$^{-/-}$ mice and their wild-type littermates were subjected to DEN one time at 15-day age, and they were consistently given hepatotoxin CCl_4 injections starting at four weeks of age (**Figure 3A**). This model revealed representative features of human HCC development, reflected the multiple stages of hepatocarcinogenesis, and faithfully recapitulated the natural history of HCC, including chronic injury, inflammation, and fibrosis. *Gpr110*$^{-/-}$ mice showed an obvious diminution of tumor number and tumor load after DEN plus CCl_4 injections (**Figure 3B-D**). As expected, H&E staining and immunostaining of anti-alpha fetoprotein (AFP) antibody definitely confirmed that the tumors were hepatocellular carcinoma in the *Gpr110*$^{-/-}$ mice and wild-type mice (**Figure 3E**). The survival curves revealed that the survival of *Gpr110*$^{-/-}$ mice was apparently longer than that of wild-type mice (P<0.05, **Figure 3F**). As illustrated in **Figure 3G**, after four months of CCl_4 treatment only a 20% occurrence rate was observed in the surface of livers in the *Gpr110*$^{-/-}$ mice, whereas nearly 100% of Gpr110 wild-type mice had developed single- or multiple-surface nodular tumors. Moreover, deletion of *Gpr110* in tumor tissue masses significantly reduced tumor growth in the nude mice tumor xenograft model (Supplementary Figure 8). Tumor tissue masses from *Gpr110*$^{-/-}$ mice and wild-type mice were subcutaneously inoculated into nude mice, a month later, we found that tumor tissue masses from the wild-type mice were completely developed, while tumor tissue masses from *Gpr110*$^{-/-}$ mice had all disappeared. These tumors were well delineated and exhibited enlargement of hepatocytic plates, disruption of the reticulin network, and absence of portal tracts. Sirius red staining showed less severe liver fibrosis in *Gpr110*$^{-/-}$ mice (**Figure 3H**, **3I**). However, disruption of *Gpr110* did not affect the proliferation, apoptosis, vascularization and inflammation of tumors in vivo (Supplementary Figures 9 and 10). Furthermore, overexpression of GPR110 did not affect the proliferation, migration, or invasion of the human hepatocellular carcinoma cell lines SMMC-7721 or Huh7 in vitro (Supplementary Figure 11). The above findings indicate that Gpr110 may not regulate the growth of liver tumor cells, but that it accelerates injury-driven liver tumor initiation. They also suggest that Gpr110-related hepatocarcinogenesis is associated with chronic liver injury and fibrosis. Absence of *Gpr110* decelerates liver fibrosis/cirrhosis from progressing into tumorigenesis.

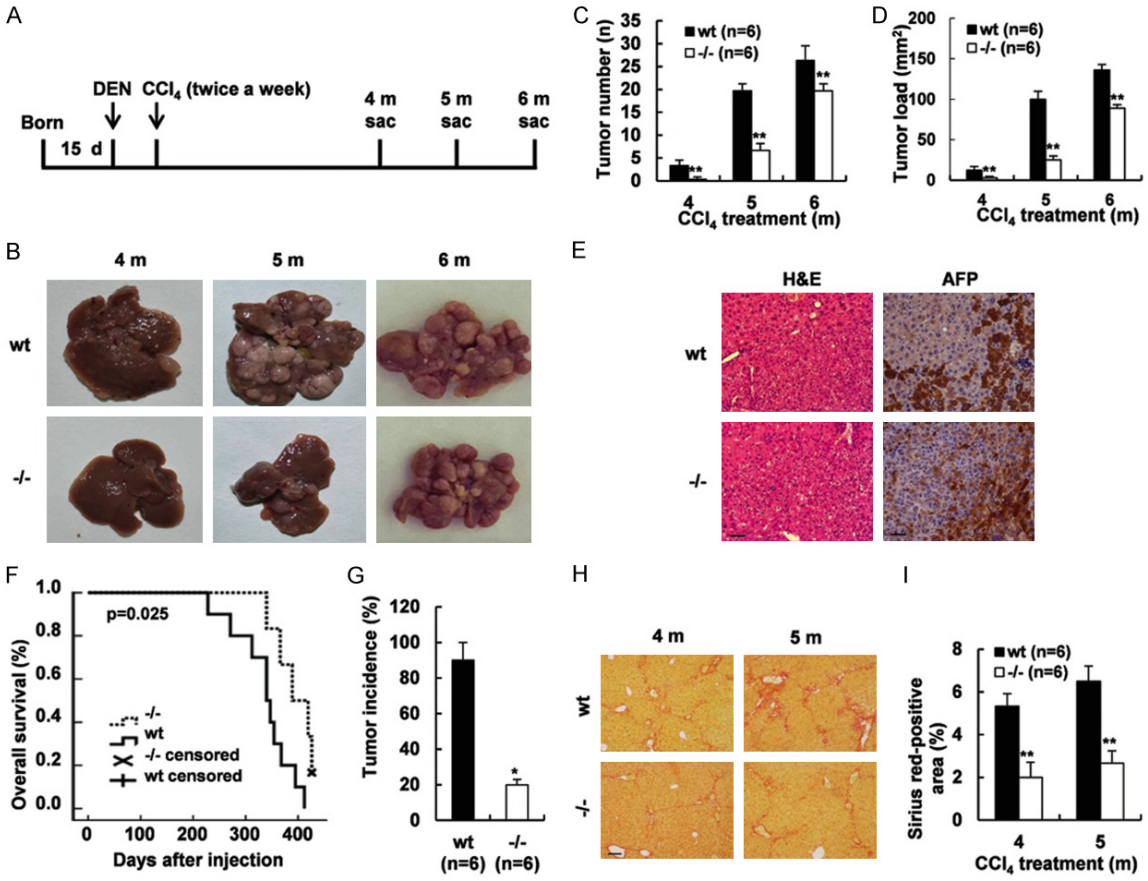

Figure 3. Deletion of *Gpr110* decelerated hepatocarcinogenesis in chronically injured livers. (A) Schematic diagram of the progression of DEN plus CCl_4-induced mouse HCC model. (B) Macroscopic liver appearance of *Gpr110*$^{-/-}$ mice and wild-type littermates injected with DEN plus CCl_4 at different time points (n=6). (C, D) Statistical analysis of Tumor number and Tumor load about *Gpr110*$^{-/-}$ mice and wild-type littermates injected with DEN plus CCl_4 at different time points (n=6) Values are presented as mean ± SD. **P*<0.05; **P<0.01. (E) H&E staining and immunohistochemical staining of AFP in tumor area about liver sections from *Gpr110*$^{-/-}$ mice and wild-type littermates injected with DEN plus CCl_4 after 5 months. Scalebar, 50 μm. (F) The survival curves of *Gpr110*$^{-/-}$ mice (n=10) and control littermates (n=7) (*P*<0.05) after DEN+CCl_4 treated. (G) After 4 months CCl_4 treated *Gpr110*$^{-/-}$ mice (n=6) and control littermates (n=6), Tumor incidence was determined and statistical analyzed (*P*<0.05). (H, I) Liver sections from (b) were collected for Sirius red staining (100×) (H). Scalebar, 100 μm. Quantified and statistical analyzed (I). Values are presented as mean ± SD. **P*<0.05; **P<0.01.

Gpr110 deficiency resulted in increased IL-6/STAT3 pathway activation in mice liver tumor

To explore the possible mechanism for the decreased susceptibility of *Gpr110*$^{-/-}$ mice to carcinogen-induced carcinogenesis, we detected several typical pathways involved in carcinogenesis as well as belonging to the GPCR pathway. Although CCl_4 induced activation of MEK, ERK, NF-kB, JNK, and p38/MAPK, there were no differences to be distinguished between the *Gpr110*$^{-/-}$ mice and control littermates (Supplementary Figure 12). Interestingly, we detected obvious enhanced activation of STAT3 and increased IL-6 secretion in the liver tumors from DEN plus CCl_4-treated *Gpr110*$^{-/-}$ mice (**Figure 4A-C**). It has been reported that activation of STAT3 in hepatocytes plays a protective role in preventing liver tumorigenesis induced by chronic CCl_4 challenge [24]. Meanwhile, transient overexpression of GPR110 in the transfected human hepatocellular carcinoma cell lines SMMC-7721 and Huh-7 inhibited IL-6 expression and STAT3 activation (**Figure 4D-F**). Thus, these results suggest that Gpr110 deficiency leads to increased IL-6/STAT3 pathway activation in mice liver tumor and enhanced IL-6/STAT3 pathway activation in *Gpr110*$^{-/-}$ mice liver

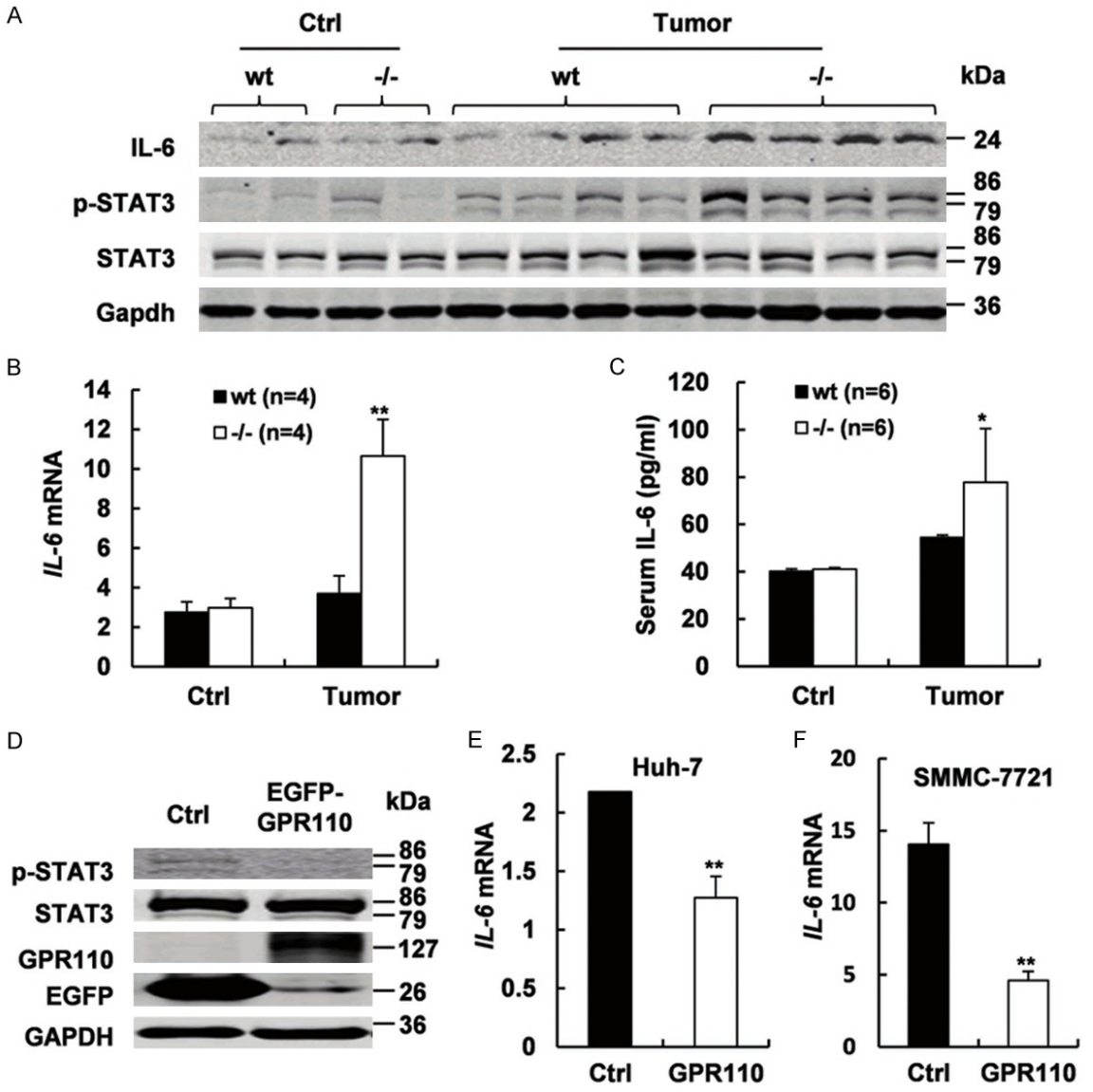

Figure 4. *Gpr110*$^{-/-}$ mice exhibited sustained increased IL-6/STAT3 pathway activation in liver tumors. A. Immunoblot staining analysis of IL-6, p-STAT3, and total STAT3 in olive oil and DEN plus CCl_4-treated 5 month *Gpr110*$^{-/-}$ mice and wild-type littermate mice liver (n=6). B. qRT-PCR analysis of *IL-6* expression in olive oil and DEN plus CCl_4-treated 5 months *Gpr110*$^{-/-}$ mice and wild-type littermate mice livers (n=4). Values are presented as mean ± SD from three independent experiments. **P*<0.05; **P<0.01. C. ELISA analysis of serum levels of IL-6 in olive oil and DEN plus CCl_4-treated 5 months *Gpr110*$^{-/-}$ mice and wild-type littermate mice livers (n=4). Values are presented as mean ± SD. **P*<0.05; **P<0.01. D. Western blot analysis of GFP, p-STAT3, and total STAT3 in Huh-7 and SMMC-7721 cells after instantaneous overexpression of GPR110. E, F. qRT-PCR analysis of *IL-6* expression in Huh-7 and SMMC-7721 cells after instantaneous overexpression of GPR110. Values are presented as mean ± SD from three independent experiments. **P*<0.05; **P<0.01.

most likely contributes to decelerate tumorigenesis after DEN plus CCl_4 exposure.

Increased IL-6/STAT3 pathway activation was detected during liver injury and fibrosis in Gpr110$^{-/-}$ *mice*

Subsequently, we investigated whether IL-6/STAT3 pathway persistently activated in the early stage of CCl_4 induced liver injury and fibrosis in *Gpr110*$^{-/-}$ mice. Interleukin-6 (IL-6), an important pro-inflammatory cytokine, was found to be higher in *Gpr110*$^{-/-}$ mice during liver injury and fibrosis (**Figure 5A-F**). Constantly increased STAT3 activation was also detected in the hepatocytes of the *Gpr110*$^{-/-}$ group after CCl_4 treatment (**Figure 5G**, **5H**). As

well as, we assessed a few of classical STAT3 target genes, *Mcl-1*, *Socs*, *FOXO3A*, *FOXO1*, *Pim-1* and *c-Myc* by real-time PCR, except for *Pim-1* and *c-Myc*, the others were all higher expressed in Gpr110$^{-/-}$ mice after 24 h CCl_4 treatment (**Figure 5I**). Interleukin-6 (IL-6) has been shown to be a hepatoprotective cytokine in this model [25], as well as in several other liver injury models, including ischemia/reperfusion, partial hepatectomy, alcoholic and nonalcoholic fatty liver, and Con A-induced T cell hepatitis model [26, 27]. Numerous studies have demonstrated the hepatoprotective role of IL-6 against liver injury, despite its pro-inflammatory effect [28, 29]. The hepatoprotective effects of IL-6 are mediated mainly via activation of signal transducers and activators of transcription 3 (STAT3) in the hepatocytes [26]. The IL-6/STAT3 pathway has been shown to exert hepatoprotective effects during liver injury, fibrosis and hepatocarcinogenesis by regulating the expression of a wide array of genes, including anti-apoptotic and anti-oxidative genes that protect against hepatocyte damage [24, 30]. In summary, these results suggest that a persistently enhanced IL-6/STAT3 pathway activation due to deletion of Gpr110 is most likely to alleviate hepatocellular damage and fibrosis and delay the development of cirrhosis and progression into HCC.

Phospho-STAT3 inhibitor restored the sensitivity of Gpr110$^{-/-}$ mice to CCl_4-induced liver fibrosis and carcinogenesis

As *Gpr110$^{-/-}$* mice displayed persistently increased IL-6/STAT3 activation during CCl_4 treatment, and IL-6/STAT3 exerted a hepatoprotective function during CCl_4 challenge, it seemed likely to account for the decreased susceptibility of *Gpr110$^{-/-}$* mice to CCl_4-induced liver fibrosis and hepatocarcinogenesis. To test this hypothesis, we treated both groups with four weeks of CCl_4 with or without a specific phospho-STAT3 inhibitor, Stattic [31]. Correspondingly, activation of STAT3 was inhibited, and liver fibrosis in *Gpr110$^{-/-}$* mice were more severe than that in control mice after long-termCCl_4 plus Stattic treatment (**Figure 6A-C**). During the process of DEN plus CCl_4-induced hepatocarcinogenesis, simultaneously injected with Stattic, phospho-STAT3 levels in *Gpr110$^{-/-}$* group distinctly declined (**Figure 6D**). As anticipated, liver cancers in *Gpr110$^{-/-}$* mice were completely accelerated, and liver cirrhosis was seriously exacerbated (**Figure 6E-G**). Taken together, this implies that deletion of *Gpr110* increases IL-6/STAT3 activation, which protects against CCl_4-induced hepatocyte damage, cirrhosis, and decelerates malignant transformation (**Figure 6H**).

Discussion

HCC carcinogenesis is an intricate process that usually develops from chronic liver injury, hepatocyte regeneration, and cirrhosis. It is triggered by a variety of etiologic factors, dysregulations of related signal pathways, and genetic alterations, eventually leading to malignant transformation and carcinogenesis [32, 33]. So far, many scientific studies have focused on the possible mechanisms involved in the progression from premalignant lesions to overt carcinomas. However, the intercessors that are responsible for a high risk of developing HCC in a chronically injured liver remain to be fully explored.

GPR110 has been identified as a proto-oncogene, and has also shown high expression levels in lung and prostate cancer, suggesting that it plays a role in tumor pathology. In our study, we found DEN plus CCl_4 treatment resulted in fewer dysplastic nodules in *Gpr110$^{-/-}$* mice than in their wild-type littermates. This strategy of induced liver cancer, which recapitulates human HCC development, can reflect the multiple stages of hepatocarcinogenesis, which including continuous DNA damage, fibrogenesis, cirrhosis, and tumor formation. Therefore, the restraint of carcinogen-induced hepatocarcinogenesis by *Gpr110* deficency may be of the result of weakening persistent hepatocyte damage and fibrosis in the microenvironment.

The hepatotoxicity of CCl_4 is mediated by the direct induction of hepatocellular injury and necrosis. Once CCl_4 is injected, the cytochrome p450 (CYP2E1) in hepatocytes metabolizes it into trichloromethyl radicals (CCl_3*), which elicit the production of reactive oxygen intermediates and then cause lipid peroxidation and membrane damage [19]. Repeated and prolonged administration of CCl_4 for up to two years induces 50% HCC carcinogenesis in mice [34, 35]. Moreover, tumors developed using this strategy displayed typical features of human HCC. CCl_4 can induce hepatocytic

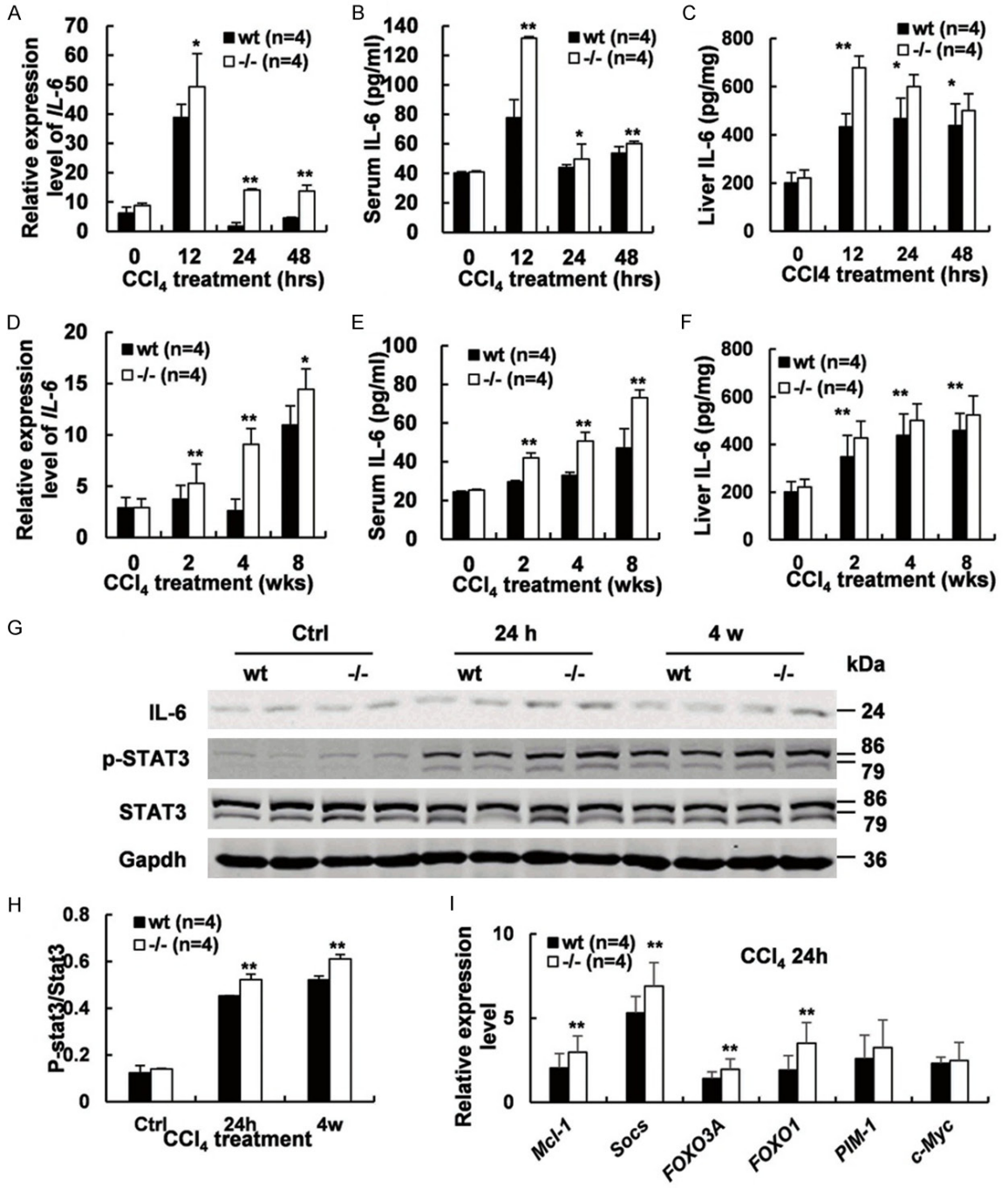

Figure 5. Enhanced IL-6/STAT3 pathway activation was detected in *Gpr110*$^{-/-}$ mice during liver injury and fibrosis. (A-C) qRT-PCR, ELISA analysis of serum levels of IL-6 and ELISA analysis of liver levels of IL-6 expression in *Gpr110*$^{-/-}$ mice and wild-type littermates treated with CCl_4 for 0, 12, 24, and 48 hours (n=4). Values are presented as mean ± SD from three independent experiments. *P<0.05; **P<0.01. (D-F) qRT-PCR, ELISA analysis of serum levels of IL-6 and ELISA analysis of liver levels of IL-6 expression in *Gpr110*$^{-/-}$ mice and wild-type littermates treated with CCl_4 for 0, 2, 4, and 8 weeks (n=4). Values are presented as mean ± SD from three independent experiments. *P<0.05; **P<0.01. (G) Immunoblot staining analysis of IL-6, p-STAT3, and total STAT3 in *Gpr110*$^{-/-}$ mice and wild-type littermate liver treated with CCl_4 for 0 h, 24 h and four weeks. (H) Quantification and statistical analysis of STAT3 activation detected by Immunoblot staining in (G). Values are presented as mean ± SD. *P<0.05; **P<0.01. (I) qRT-PCR analysis of classical STAT3 target genes, *Mcl-1*, *Socs*, *FOXO3A*, *FOXO1*, *Pim-1* and *c-Myc* in Gpr110$^{-/-}$ mice and wild-type littermate liver treated with CCl_4 for 24 h. Values are presented as mean ± SD from three independent experiments. *P<0.05; **P<0.01.

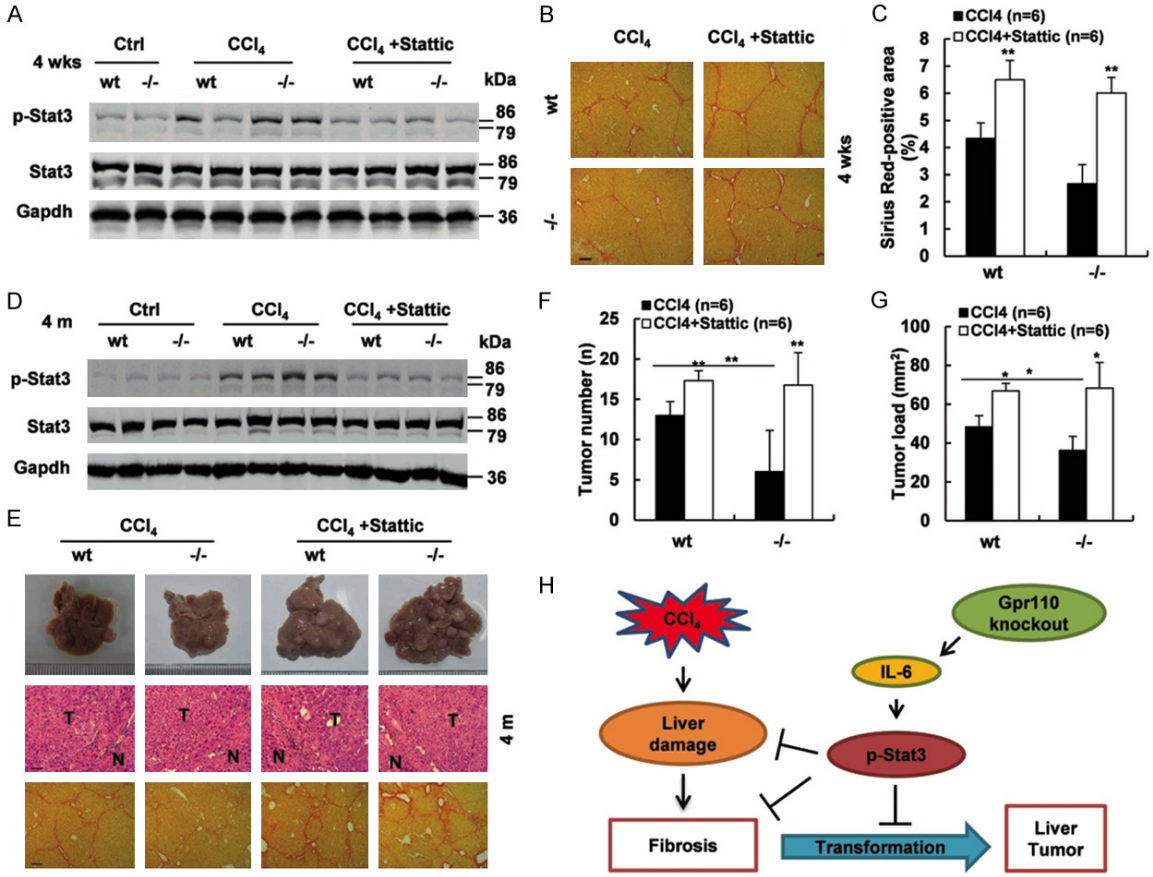

Figure 6. p-STAT3 inhibitor promoted liver fibrosis and carcinogenesis in *Gpr110*$^{-/-}$ mice after CCl_4 exposure. (A) Immunoblot staining analysis of p-STAT3 and total STAT3 in Gpr110$^{-/-}$ mice and wild-type littermate liver. Mice were treated with CCl_4 and CCl_4 plus Stattic for four weeks (n=6). (B, C) Sirius red staining of liver sections from (a) (100×) (B). Scalebar, 100 μm. Quantifications and statistical analysis (C). Values are presented as mean ± SD. **P*<0.05; **P<0.01. (D) Immunoblot staining analysis of p-STAT3 and total STAT3 in DEN plus CCl_4 and DEN plus CCl_4 plus Stattic-treated Gpr110$^{-/-}$ mice and wild-type mice livers (n=6). (E) Macroscopic liver appearance of *Gpr110*$^{-/-}$ mice and wild-type littermates. H&E (200×). Scalebar, 50 μm. Sirius red staining (100×) of mice treated with CCl_4 or CCl_4 plus Stattic for four months. Scalebar, 100 μm. (F, G) Tumor number and Tumor load from (E) were quantified and statistical analyzed (n=6). Values are presented as mean ± SD. **P*<0.05; **P<0.01. (H) Schematic representation of the function and potential mechanism of Gpr110 in liver malignant transformation.

death, and the surviving hepatocytes undergo compensatory proliferation. Reduced proliferation of hepatocytes was found in *Gpr110*$^{-/-}$ mice compared to wild-type mice after CCl_4 stimulation, which was consistent with a smaller necrosis area in *Gpr110*$^{-/-}$ mice compared to their wild-type littermates. Because compensatory proliferation is critical for tumor development, the most likely interpretation of our results is that disruption of *Gpr110* inhibited malignant transformation of liver cirrhosis by decreased compensatory growth in the microenvironment of inflammation and fibrillation.

In general, liver injury is accompanied by inflammation, which is generally believed to play a key role in accelerating the progression of liver damage. However, clinical data revealed that inflammation was not always consistent with hepatocellular damage in some patients. We showed that inflammation may attenuate liver necrosis induced by CCl_4 in *Gpr110*$^{-/-}$ mice. Such a mechanism was associated with a hepatoprotective cytokine, IL-6, and IL-6/STAT3 pathway increased activation. IL-6 has been shown to be a hepatoprotective cytokine in this liver injury model.

The IL-6/STAT3 pathway was observed to be constantly increased in the *Gpr110*$^{-/-}$ group after CCl_4 treatment.IL-6 is a pleiotropic cytokine with beneficial effects for the liver;

numerous studies have demonstrated the hepatoprotective role of IL-6 against liver injury despite its pro-inflammatory effect [28, 29]. IL-6 knockout mice were reported to be more susceptible to CCl_4-induced liver injury and fibrosis [25]. Other studies have demonstrated that liver fibrosis was reduced in IL-6-deficient mice after CCl_4 treatment [36, 37]. The hepatoprotective effect of hepatic STAT3 has been well documented in various models of liver injury [22, 30, 38, 39]. Our postulation was that disruption of *Gpr110*increased activation of the IL-6/STAT3 pathway, which protected against hepatic damage and fibrosis induced by CCl_4, consequently suppressing injury-driven liver tumor initiation. In addition, a specific phospho-STAT3 inhibitor significantly blocked disruption of *Gpr110*-mediated IL-6/STAT3 activation, and promoted hepatic fibrosis and HCC formation. Gpr110 is very likely involved in CCl_4-induced IL-6/STAT3 pathway activation.

There is mounting evidence that adhesion GPCRs can couple to G proteins to activate a variety of different downstream signaling pathways. Therefore, disruption of *Gpr110* may lead to the dysregulation of GPCR's downstream signaling pathways and relevant molecules which are associated with tumorigenesis. Although CCl_4 induced ERK, NF-kB, JNK, and p38/MAPK activation, almost no differences between the *Gpr110*$^{-/-}$ mice and control mice indicated that these pathways were not involved.

It has been well established that almost 90% of HCC cases develop as a result of cirrhosis in clinical practice [3, 40]. Now, a number of primary treatment options, such as antiviral therapy and weight loss strategies, are variably effective for the prevention of HCC. Unfortunately, a significant number of patients still progress to end-stage liver disease. Thus, it is urgently necessary for new therapeutic strategies to be developed for the prevention or treatment of hepatic fibrosis, cirrhosis, and HCC. Our results demonstrated the significance of Gpr110 by regulating IL-6/STAT3 to allay cirrhosis and decelerate injury-driven liver tumor initiation, and suggested that targeting GPR110 and IL-6/STAT3 activation has the potential for liver disease therapy. Recently, a new strategy targeting multiple GPCRs was proposed for cancer treatment. In light of our studies, a combination of targeting GPR110 and IL-6/STAT3 activation may profoundly improve liver cirrhosis therapies. Further studies are needed to investigate the way by which Gpr110, as a receptor, regulates the secretion of IL-6, as well as the activation of the IL-6/STAT3 signaling pathway.

Acknowledgements

We thank Shanghai Research Center for Model Organisms for the generation of *Gpr110* knockout mice. This work was partially supported by grants from National Natural Science Foundation of China (81430028, 81502383), the Ministry of Science and Technology of China (2011BAI15B02), the grants from the Science and Technology Commission of Shanghai Municipality (13DZ2280600, 15DZ2290800), and the E-Institutes of Shanghai Municipal Education Commission (E03003).

Disclosure of conflict of interest

None.

Abbreviations

HCC, hepatocellular carcinoma; ALT, alanine transaminase; AST, aspartate transaminase; DEN, diethylnitrosamine; CCl_4, carbon tetrachloride; TUNEL, terminal-deoxynucleotidyl transferase mediated nick end labeling; BrdU, 5-bromodeoxyuridine; CCR2, CC chemokine receptor 2; α-SMA, α-smoothmuscle actin; AFP, alpha fetoprotein; IL-6, interleukin-6; STAT3, signal transducer and activator of transcription; mRNA, messenger RNA; qRT-PCR, quantitative reverse transcription polymerase chain reaction.

Address correspondence to: Zhugang Wang, Research Center for Experimental Medicine of Rui-Jin Hospital Affiliated to Shanghai Jiao Tong University School of Medicine (SJTUSM), 197 Rui-Jin Road II, Building #17, Shanghai 200025, China. Tel: +86 21 64457997; Fax: +86 21 64457997; E-mail: zhugangw@shsmu.edu.cn

References

[1] Llovet JM, Burroughs A and Bruix J. Hepatocellular carcinoma. Lancet 2003; 362: 1907-1917.

[2] Mu X, Espanol-Suner R, Mederacke I, Affo S, Manco R, Sempoux C, Lemaigre FP, Adili A, Yuan D, Weber A, Unger K, Heikenwalder M, Leclercq IA and Schwabe RF. Hepatocellular

carcinoma originates from hepatocytes and not from the progenitor/biliary compartment. J Clin Invest 2015; 125: 3891-3903.
[3] El-Serag HB and Rudolph KL. Hepatocellular carcinoma: epidemiology and molecular carcinogenesis. Gastroenterology 2007; 132: 2557-2576.
[4] Friedman SL. Evolving challenges in hepatic fibrosis. Nat Rev Gastroenterol Hepatol 2010; 7: 425-436.
[5] Bjarnadottir TK, Fredriksson R, Hoglund PJ, Gloriam DE, Lagerstrom MC and Schioth HB. The human and mouse repertoire of the adhesion family of G-protein-coupled receptors. Genomics 2004; 84: 23-33.
[6] Fredriksson R, Lagerstrom MC, Lundin LG and Schioth HB. The G-protein-coupled receptors in the human genome form five main families. Phylogenetic analysis, paralogon groups, and fingerprints. Mol Pharmacol 2003; 63: 1256-1272.
[7] Bjarnadottir TK, Fredriksson R and Schioth HB. The adhesion GPCRs: a unique family of G protein-coupled receptors with important roles in both central and peripheral tissues. Cell Mol Life Sci 2007; 64: 2104-2119.
[8] Nishimori H, Shiratsuchi T, Urano T, Kimura Y, Kiyono K, Tatsumi K, Yoshida S, Ono M, Kuwano M, Nakamura Y and Tokino T. A novel brain-specific p53-target gene, BAI1, containing thrombospondin type 1 repeats inhibits experimental angiogenesis. Oncogene 1997; 15: 2145-2150.
[9] Vallon M and Essler M. Proteolytically processed soluble tumor endothelial marker (TEM) 5 mediates endothelial cell survival during angiogenesis by linking integrin alpha(v) beta3 to glycosaminoglycans. J Biol Chem 2006; 281: 34179-34188.
[10] Hatanaka H, Oshika Y, Abe Y, Yoshida Y, Hashimoto T, Handa A, Kijima H, Yamazaki H, Inoue H, Ueyama Y and Nakamura M. Vascularization is decreased in pulmonary adenocarcinoma expressing brain-specific angiogenesis inhibitor 1 (BAI1). Int J Mol Med 2000; 5: 181-183.
[11] Lee JH, Koh JT, Shin BA, Ahn KY, Roh JH, Kim YJ and Kim KK. Comparative study of angiostatic and anti-invasive gene expressions as prognostic factors in gastric cancer. Int J Oncol 2001; 18: 355-361.
[12] Carson-Walter EB, Watkins DN, Nanda A, Vogelstein B, Kinzler KW and St Croix B. Cell surface tumor endothelial markers are conserved in mice and humans. Cancer Res 2001; 61: 6649-6655.
[13] Shashidhar S, Lorente G, Nagavarapu U, Nelson A, Kuo J, Cummins J, Nikolich K, Urfer R and Foehr ED. GPR56 is a GPCR that is overexpressed in gliomas and functions in tumor cell adhesion. Oncogene 2005; 24: 1673-1682.
[14] Lin HH. Adhesion family of G protein-coupled receptors and cancer. Chang Gung Med J 2012; 35: 15-27.
[15] Lum AM, Wang BB, Beck-Engeser GB, Li L, Channa N and Wabl M. Orphan receptor GPR110, an oncogene overexpressed in lung and prostate cancer. BMC Cancer 2010; 10: 40.
[16] Dapito DH, Mencin A, Gwak GY, Pradere JP, Jang MK, Mederacke I, Caviglia JM, Khiabanian H, Adeyemi A, Bataller R, Lefkowitch JH, Bower M, Friedman R, Sartor RB, Rabadan R and Schwabe RF. Promotion of hepatocellular carcinoma by the intestinal microbiota and TLR4. Cancer Cell 2012; 21: 504-516.
[17] Zhao X, Fu J, Xu A, Yu L, Zhu J, Dai R, Su B, Luo T, Li N, Qin W, Wang B, Jiang J, Li S, Chen Y and Wang H. Gankyrin drives malignant transformation of chronic liver damage-mediated fibrosis via the Rac1/JNK pathway. Cell Death Dis 2015; 6: e1751.
[18] Sun H, Chen L, Zhou W, Hu L, Li L, Tu Q, Chang Y, Liu Q, Sun X, Wu M and Wang H. The protective role of hydrogen-rich saline in experimental liver injury in mice. J Hepatol 2011; 54: 471-480.
[19] Basu S. Carbon tetrachloride-induced lipid peroxidation: eicosanoid formation and their regulation by antioxidant nutrients. Toxicology 2003; 189: 113-127.
[20] Mandrekar P and Szabo G. Signalling pathways in alcohol-induced liver inflammation. J Hepatol 2009; 50: 1258-1266.
[21] Heydtmann M and Adams DH. Chemokines in the immunopathogenesis of hepatitis C infection. Hepatology 2009; 49: 676-688.
[22] Horiguchi N, Lafdil F, Miller AM, Park O, Wang H, Rajesh M, Mukhopadhyay P, Fu XY, Pacher P and Gao B. Dissociation between liver inflammation and hepatocellular damage induced by carbon tetrachloride in myeloid cell-specific signal transducer and activator of transcription 3 gene knockout mice. Hepatology 2010; 51: 1724-1734.
[23] Mofrad P, Contos MJ, Haque M, Sargeant C, Fisher RA, Luketic VA, Sterling RK, Shiffman ML, Stravitz RT and Sanyal AJ. Clinical and histologic spectrum of nonalcoholic fatty liver disease associated with normal ALT values. Hepatology 2003; 37: 1286-1292.
[24] Wang H, Lafdil F, Wang L, Park O, Yin S, Niu J, Miller AM, Sun Z and Gao B. Hepatoprotective versus oncogenic functions of STAT3 in liver tumorigenesis. Am J Pathol 2011; 179: 714-724.

[25] Kovalovich K, DeAngelis RA, Li W, Furth EE, Ciliberto G and Taub R. Increased toxin-induced liver injury and fibrosis in interleukin-6-deficient mice. Hepatology 2000; 31: 149-159.
[26] Gao B. Cytokines, STATs and liver disease. Cell Mol Immunol 2005; 2: 92-100.
[27] Jin X, Zhang Z, Beer-Stolz D, Zimmers TA and Koniaris LG. Interleukin-6 inhibits oxidative injury and necrosis after extreme liver resection. Hepatology 2007; 46: 802-812.
[28] Blindenbacher A, Wang X, Langer I, Savino R, Terracciano L and Heim MH. Interleukin 6 is important for survival after partial hepatectomy in mice. Hepatology 2003; 38: 674-682.
[29] Wuestefeld T, Klein C, Streetz KL, Betz U, Lauber J, Buer J, Manns MP, Muller W and Trautwein C. Interleukin-6/glycoprotein 130-dependent pathways are protective during liver regeneration. J Biol Chem 2003; 278: 11281-11288.
[30] Klein C, Wustefeld T, Assmus U, Roskams T, Rose-John S, Muller M, Manns MP, Ernst M and Trautwein C. The IL-6-gp130-STAT3 pathway in hepatocytes triggers liver protection in T cell-mediated liver injury. J Clin Invest 2005; 115: 860-869.
[31] Scuto A, Kujawski M, Kowolik C, Krymskaya L, Wang L, Weiss LM, Digiusto D, Yu H, Forman S and Jove R. STAT3 inhibition is a therapeutic strategy for ABC-like diffuse large B-cell lymphoma. Cancer Res 2011; 71: 3182-3188.
[32] Ding J and Wang H. Multiple interactive factors in hepatocarcinogenesis. Cancer Lett 2014; 346: 17-23.
[33] Montalto G, Cervello M, Giannitrapani L, Dantona F, Terranova A and Castagnetta LA. Epidemiology, risk factors, and natural history of hepatocellular carcinoma. Ann N Y Acad Sci 2002; 963: 13-20.
[34] Sun B and Karin M. The therapeutic value of targeting inflammation in gastrointestinal cancers. Trends Pharmacol Sci 2014; 35: 349-357.
[35] McCay PB, Lai EK, Poyer JL, DuBose CM and Janzen EG. Oxygen- and carbon-centered free radical formation during carbon tetrachloride metabolism. Observation of lipid radicals in vivo and in vitro. J Biol Chem 1984; 259: 2135-2143.
[36] Sun R, Tian Z, Kulkarni S and Gao B. IL-6 prevents T cell-mediated hepatitis via inhibition of NKT cells in CD4+ T cell- and STAT3-dependent manners. J Immunol 2004; 172: 5648-5655.
[37] Rio A, Gassull MA, Aldeguer X, Ojanguren I, Cabre E and Fernandez E. Reduced liver injury in the interleukin-6 knockout mice by chronic carbon tetrachloride administration. Eur J Clin Invest 2008; 38: 306-316.
[38] Haga S, Terui K, Zhang HQ, Enosawa S, Ogawa W, Inoue H, Okuyama T, Takeda K, Akira S, Ogino T, Irani K and Ozaki M. Stat3 protects against Fas-induced liver injury by redox-dependent and -independent mechanisms. J Clin Invest 2003; 112: 989-998.
[39] Sakamori R, Takehara T, Ohnishi C, Tatsumi T, Ohkawa K, Takeda K, Akira S and Hayashi N. Signal transducer and activator of transcription 3 signaling within hepatocytes attenuates systemic inflammatory response and lethality in septic mice. Hepatology 2007; 46: 1564-1573.
[40] Aravalli RN, Steer CJ and Cressman EN. Molecular mechanisms of hepatocellular carcinoma. Hepatology 2008; 48: 2047-2063.

Supplementary materials & methods

Wound-healing assay

Cells were grown in six-wells plates with DMEM containing 10% FBS until 90% confluence. A "wound" was made via scratching with a pipette tip. After cultured in medium without FBS for 48 h, cell migration was observed using light microscopy. The migration distance of cells at the same position was measured by using Image-Pro Plus software. All experiments were independently repeated three times.

Transwell migration assay

Cells (1×10^4) were seeded in 8-μm cell culture inserts (Corning Incorporated, Corning, NY, USA) in DMEM without FBS and incubated in 24-well plates with 10% FBS supplemented with DMEM for 16 h. Transmigration cells were stained with 0.1% crystal violet. Photographs of five randomly selected fields of the fixed cells were captured, and cells were counted. Experiments were independently repeated three times.

Xenograft model

Animal experimental protocols were approved by the Animal Care and Use Committee of Shanghai Jiao Tong University School of Medicine. Six- week-old male nude mice (BALB/c) were housed six mice per cage in a specific pathogen-free room with a 12-hr light/dark schedule at 25°C±1°C and were fed an autoclaved chow diet and water ad libitum. The mice were randomly divided into indicated groups (6-8 mice/group) before inoculation, Tumor tissue masses from *Gpr110*$^{-/-}$ mice and wild-type mice were subcutaneously injected into the mice to form the subcutaneous model, the volume of every mass is about 2 mm^3 and one nude mouse was injected two masse, tumor growth was monitored every 4 days. Mice were sacrificed after one month and their tumor were removed. Tumor were fixed with paraform aldehyde (4%) before dehydration and embedding in paraffin. Paraffin sections were stained with H&E according to standard protocols.

Statistics

Values presented were expressed as mean ± SD. After acquiring all data for histological parameters and in vitro assays, Student's t-test was applied to determine statistical significance. All statistical tests were two-sided. A value of $p<0.05$ was considered significant.

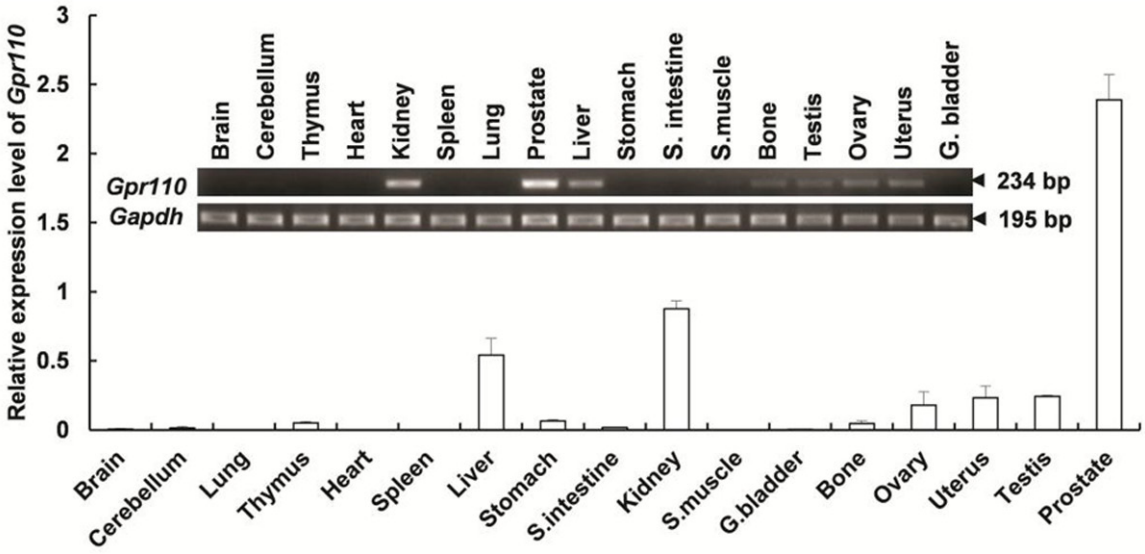

Supplementary Figure 1. Expression profile of *Gpr110* in mice. Semi-quantitative and real-time reverse transcription (RT)-PCR analyses of various mouse tissues. The highest expression level of *Gpr110* mRNA was found in the prostate, while relatively low but detectable expression levels were also observed in the kidney and liver tissues, implicating the tissue compartments where Gpr110 could execute its physiological functions in mice.

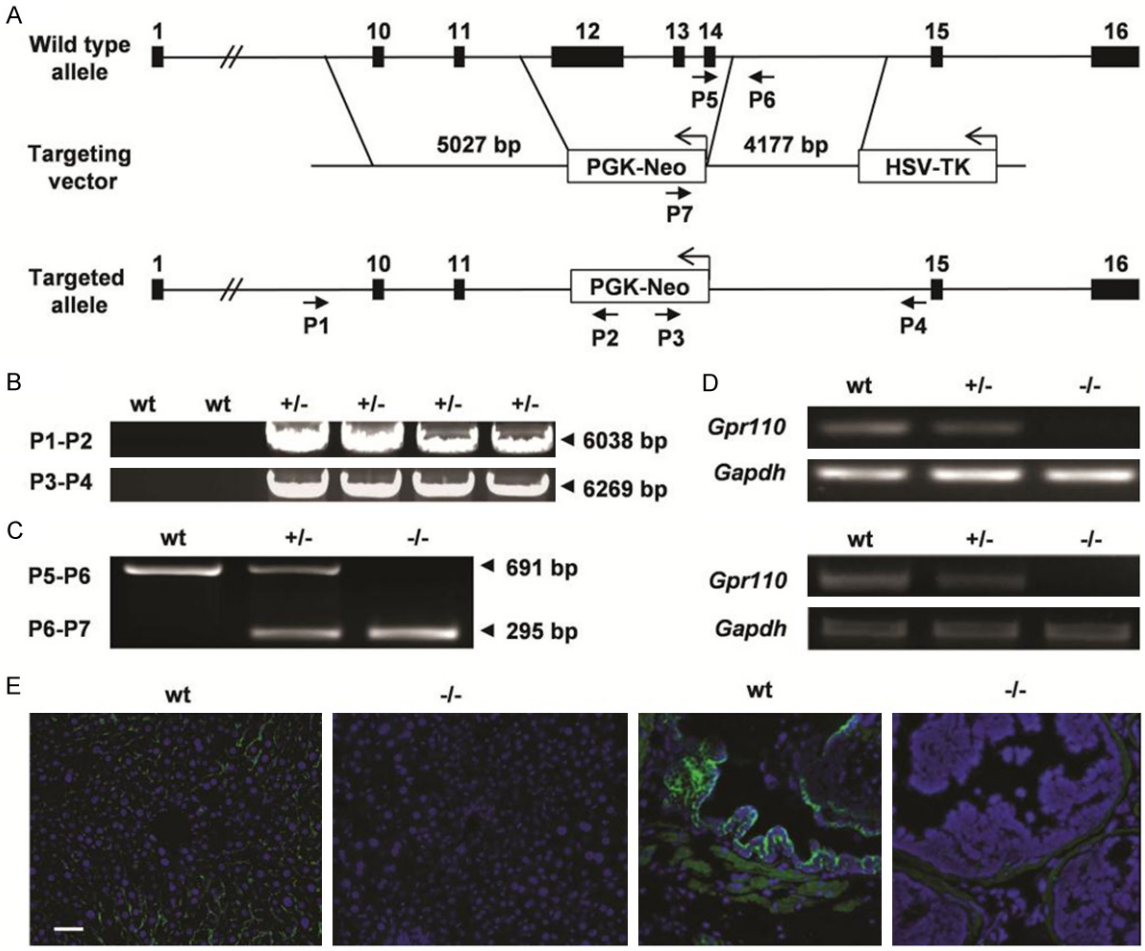

Supplementary Figure 2. Generation of *Gpr110* knockout mice. A. This is the graphic representation of the Gpr110 gene knockout strategy for the deletion of Gpr110 exon 12 to exon 14 in embryonic stem cells. Exons are shown in boxes. The targeting vector was designed to delete exon 12 to exon 14. The targeting vector contained a 5.0 kb 5' arm and 4.2 kb 3' arm. PGK-Neo and HSV-TK cassettes were used for positive and negative selections, respectively. The genomic positive of the PCR primers for genotyping are indicated by arrows. B. Genomic DNA from ES cell clones was isolated and analyzed by PCR with the primers shown in panel A. The successful targeted ES cell clones can be amplified to 6.0 kb and 6.2 kb products for the 5' arm and 3' arm, respectively. C. The PCR analysis for the genotyping of wild-type, *Gpr110*$^{+/-}$ and *Gpr110*$^{-/-}$ mice, showing PCR products of 691 bp from wild-type and 295 bp from targeted alleles. D. Absence of Gpr110 mRNA in the liver tissues (upper panel) and prostate tissues (lower panel) of wild-type, *Gpr110*$^{+/-}$ and *Gpr110*$^{-/-}$ mice detected by using RT-PCR analyses. E. Absence of Gpr110 protein in the liver tissues (left panel) and prostate tissues (right panel) of wild-type and *Gpr110*$^{-/-}$ mice detected by using immunofluorescence analyses. Scale bar, 50 μm.

Supplementary Table 1. Primer pairs for qRT-PCR

Species	Primers	Forward	Reverse
Human	IL-6	CTTCGGTCCAGTTGCCTTCT	GTGCCTCTTTGCTGCTTTCA
	GPR110	ACGCAACCTAGCAATACC	AGCAGCACCACAACGAA
	GAPDH	TGGTATCGTGGAAGGACTCATGAC	ATGCCAGTGAGCTTCCCGTTCAGC
	β-ACTIN	CTGGAACGGTGAAGGTGACA	AAGGGACTTCCTGTAACAATGCA
Mouse	Gpr110	GGGGCTTTGGCATAGGAA	TCGGCTGAGTAACTGTATCTGAGGC
	IL-6	CTTCGGTCCAGTTGCCTTCT	GTGCCTCTTTGCTGCTTTCA
	TNF-α	TCTCATTCCTGCTTGTGGC	CACTTGGTGGTTTGCTACG
	Bcl-XL	GCTTAGCCCTTTTCGAGGAC	CCCACCAGGACTGGATAATG
	Bcl2	GGTGGTGGAGGAACTCTTCA	ACCTACCCAGCCTCCGTTAT
	CYP2E1	TCCCTAAGTATCCTCCGTGAC	CGTAATCGAAGCGTTTGTTG
	IL-1β	AAAAAAGCCTCGTGCTGTCG	GTCGTTGCTTGGTTCTCCTTG
	MIP2	AGTGAACTGCGCTGTCAATGC	AGGCAAACTTTTTGACCGCC
	Mcl-1	CTTATTTCTTTCGGTGCCTTTG	CCAGTCCCGTTTCGTCCTTA
	Socs	AGGGATCTTGTCCTTTGCTG	GGAGAACGTCTTGGCTATGC
	FOXO3A	CTGTCCTATGCCGACCTGA	TGTGCCGGATGGAGTTCTT
	FOXO1	TGAAGAGCGTGCCCTACT	GATTGAGCATCCACCAAGAA
	PIM-1	GCGGCGAAATCAAACTCA	CATCGTGCTCAAACGGAAT
	c-Myc	TGTATGTGGAGCGGTTTCT	GCTGTCGTTGAGCGGGTA
	CyclinD1	GCGTACCCTGACACCAATCTC	CTCCTCTTCGCACTTCTGCTC
	CyclinA	ACATTCACACGTACCTTAGGGA	CATAGCAGCCGTGCCTACA
	β-actin	GGGAAATCGTGCGTGACATT	GCGGCAGTGGCCATCTC

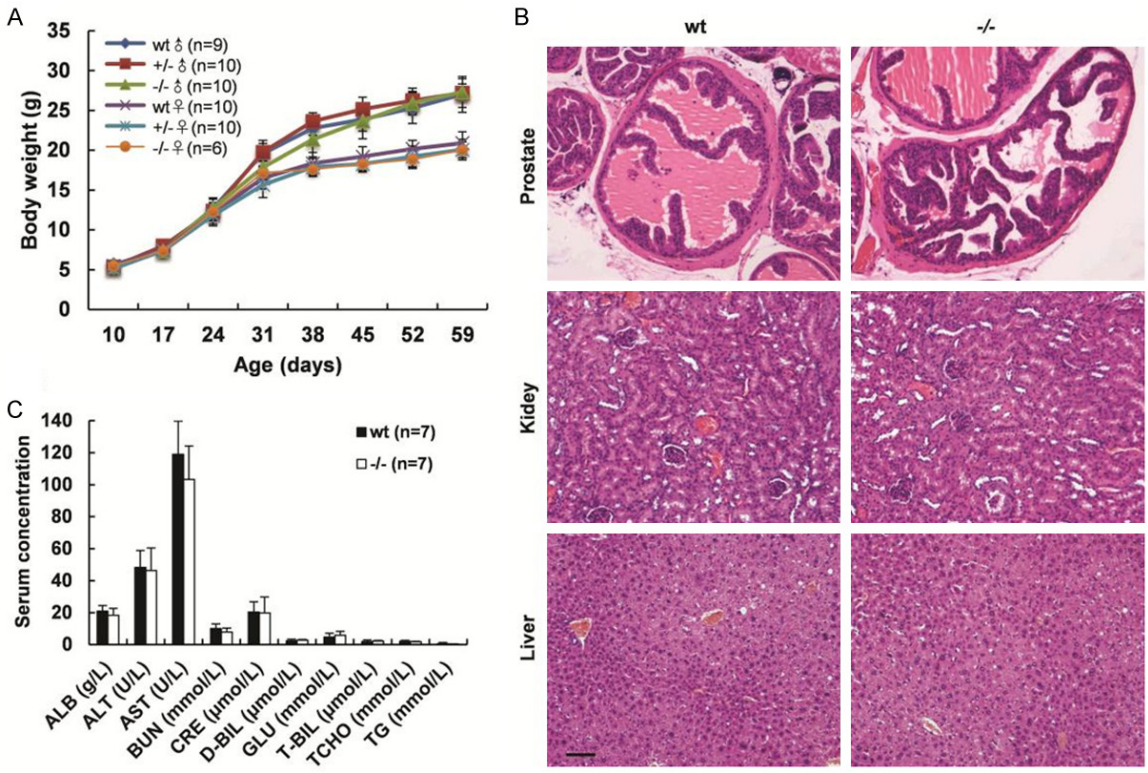

Supplementary Figure 3. *Gpr110*$^{-/-}$ mice were born alive and appeared grossly normal. A. Analysis results showed that the body weight of *Gpr110*$^{-/-}$ offspring mice had no obvious abnormalities. B. Pathological H&E staining of prostate, kidney, and liver in wild-type and Gpr110$^{-/-}$ mice. Scale bar, 100 μm. C. Serum biochemical tests of *Gpr110*$^{-/-}$ mice and wild-type mice. Values are presented as mean ± SD from three independent experiments. **p*<0.05; ***p*<0.01.

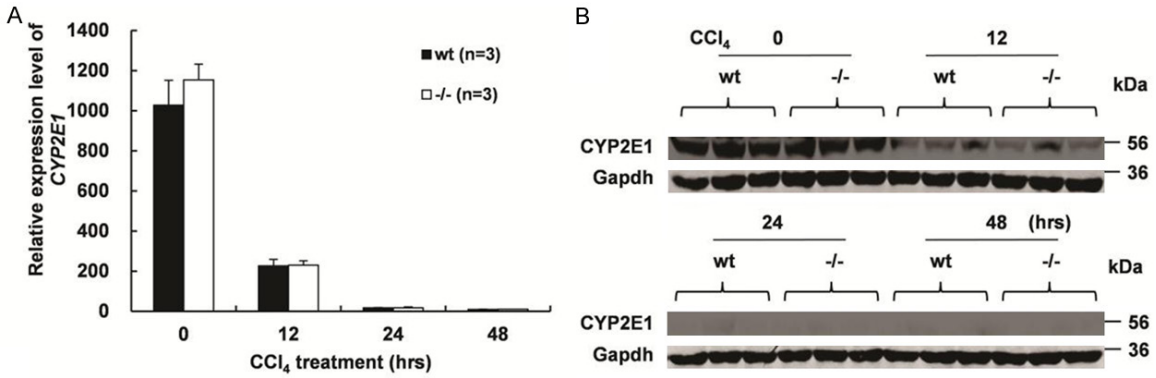

Supplementary Figure 4. The expression of CYP2E1 in liver tissues had no obvious differences between wild-type and *Gpr110*$^{-/-}$ mice. A. Real-time PCR of wild-type and *Gpr110*$^{-/-}$ mice treated with CCl_4 at different time points for expression of CYP2E1. Values are presented as mean ± SD from three independent experiments. **p*<0.05; ***p*<0.01. B. Western blot of wild-type and *Gpr110*$^{-/-}$ mice treated with CCl_4 for different time points for expression of CYP2E1.

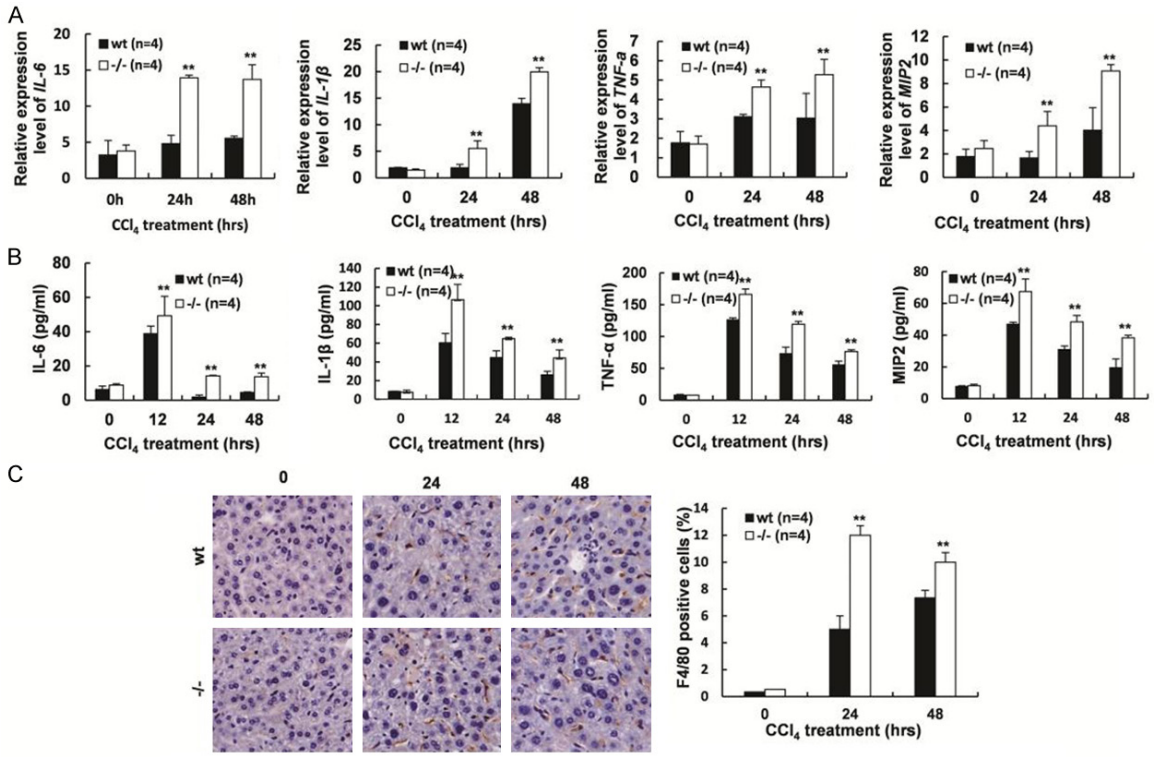

Supplementary Figure 5. Deletion of Gpr110 partially enhanced inflammation after CCl_4 induced acute liver injury. A. qRT-PCR analyses for *IL-6*, *IL-1β*, *TNF-α* and *MIP2* mRNA expression in wild-type and *Gpr110*$^{-/-}$ mice liver treated with CCl_4 for 0 h, 24 h and 48 h (n=4). Values are presented as mean ± SD from three independent experiments. **p*<0.05; ***p*<0.01. B. ELISA analysis of serum levels of IL-6, IL-1β, TNF-α and MIP2 in *Gpr110*$^{-/-}$ mice and wild-type littermates treated with CCl_4 for 0 h, 24 h and 48 h (n=4). Values are presented as mean ± SD. **p*<0.05; ***p*<0.01. C. Immunohistochemical staining of F4/80, sections from 0-, 24- and 48-hours after the CCl_4 injection-sacrificed *Gpr110*$^{-/-}$ mice and wild-type littermate liver (200×), quantified by statistical analyzing percentage of positive cells in 20 high-power fields. Values are presented as mean ± SD. **p*<0.05; ***p*<0.01.

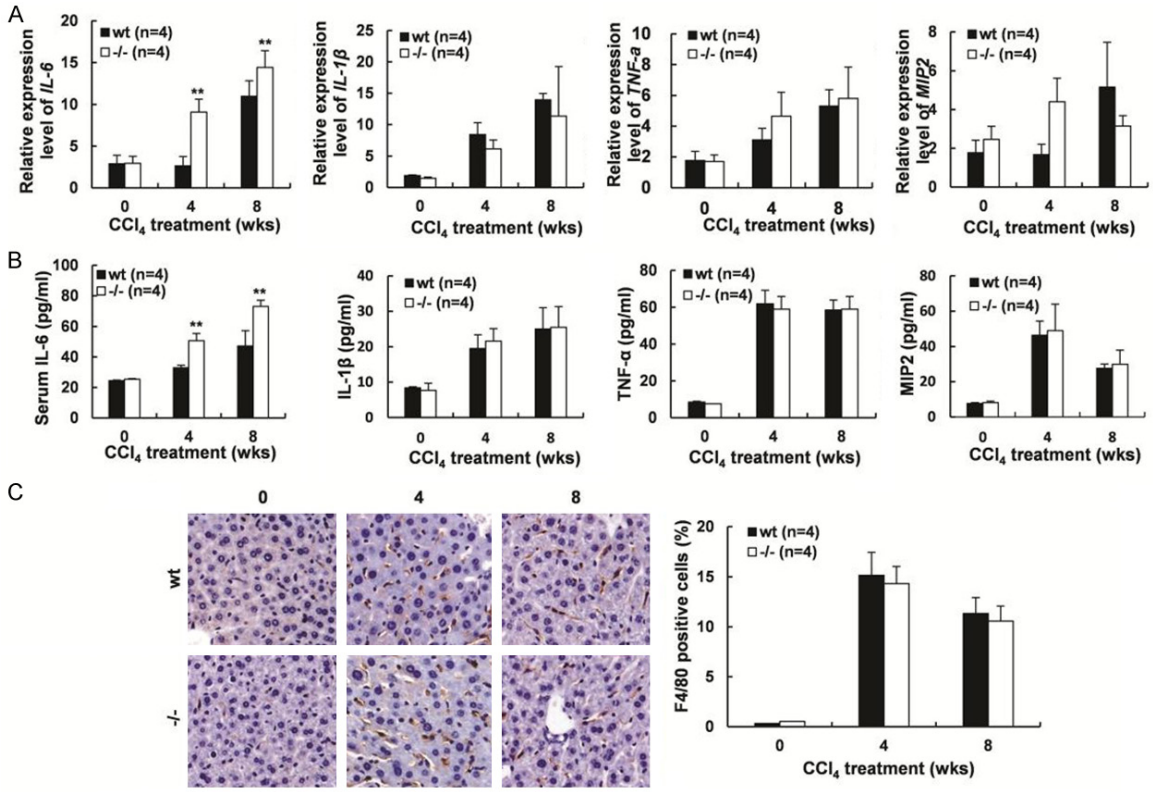

Supplementary Figure 6. Deficiency of Gpr110 did not appear affect inflammation during fibrosis induced by CCl_4. A. qRT-PCR analyses for *IL-6*, *IL-1β*, *TNF-α* and *MIP2* mRNA expression in wild-type and *Gpr110*$^{-/-}$ mice liver treated with CCl_4 for 0 week, 4 week and 8 week (n=4). Values are presented as mean ± SD from three independent experiments. **p*<0.05; ***p*<0.01. B. ELISA analysis of serum levels of IL-6, IL-1β, TNF-α and MIP2 in *Gpr110*$^{-/-}$ mice and wild-type littermates treated with CCl_4 for 0 week, 4 week and 8 week (n=4). Values are presented as mean ± SD. **p*<0.05; ***p*<0.01. C. Immunohistochemical staining of F4/80, sections from 0 week, 4 week and 8 week after the CCl_4 injection -sacrificed *Gpr110*$^{-/-}$ mice and wild-type littermate liver (200×), quantified by statistical analyzing percentage of positive cells in 20 high-power fields. Values are presented as mean ± SD. **p*<0.05; ***p*<0.01.

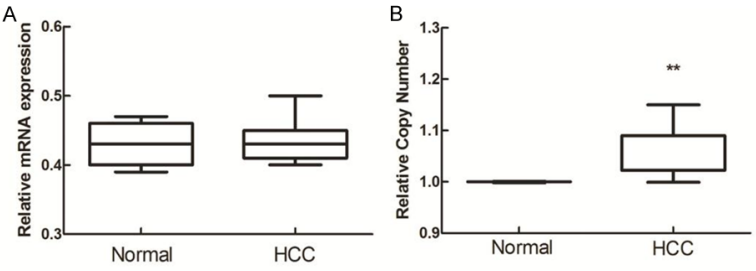

Supplementary Figure 7. The gene copy number of GPR110 rather than the expression of GPR110 in hepatocellular carcinoma was significantly different from the level in normal samples. A. Relative GPR110 mRNA expression in 225 normal and 220 hepatocellular carcinoma samples, no differential expression was observed. (TCGA database, Student t-test, p=0.276). B. Relative GPR110 gene copy number in 115 normal and 97 hepatocellular carcinoma samples, significantly differential copy number was observed. (TCGA database, Student t-test, p=9.84E-8).

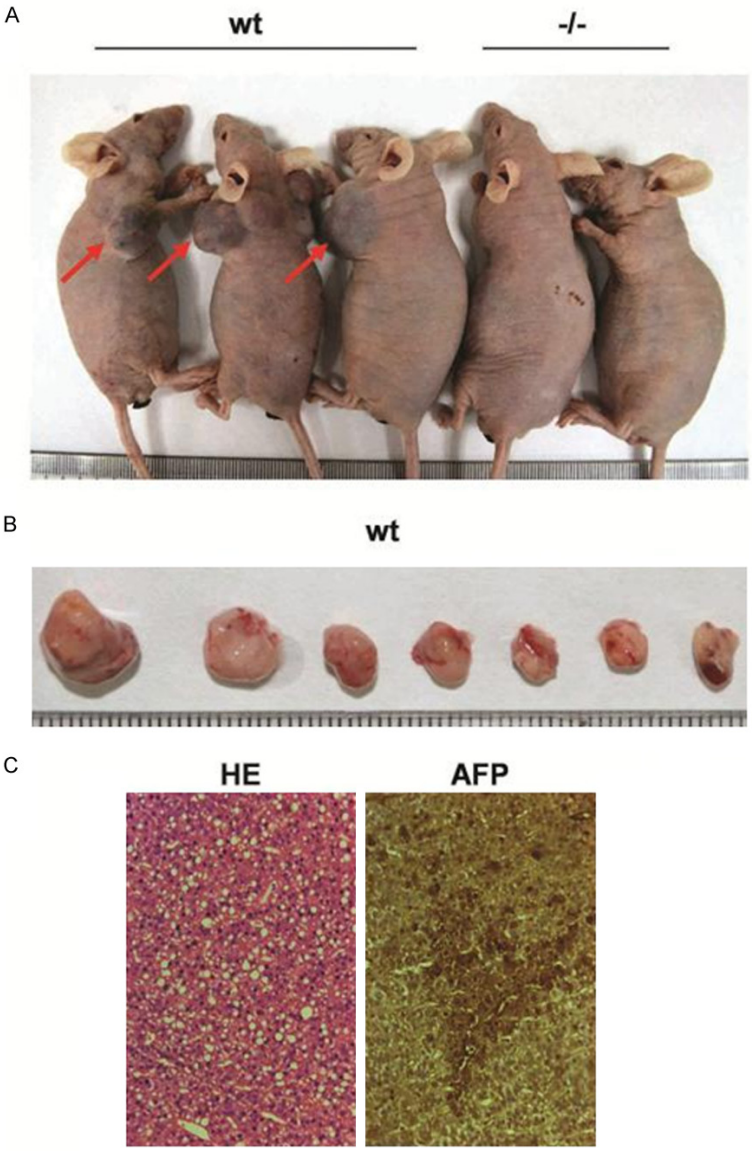

Supplementary Figure 8. Deletion of *Gpr110* in tumor tissue masses significantly reduced tumor growth in the nude mice tumor xenograft model. (A) Representative photographs of nude mice tumor xenograft, tumor tissue masses from *Gpr110*$^{-/-}$ mice (n=10), and control litter mates (n=10). (B) Tumor nodules stripping from nude mice tumor xenograft model, vaccinal tumor tissue masses from wild-type mice. (C) H&E staining of tumor sections from (B) and immunohistochemical staining of AFP in tumor area.

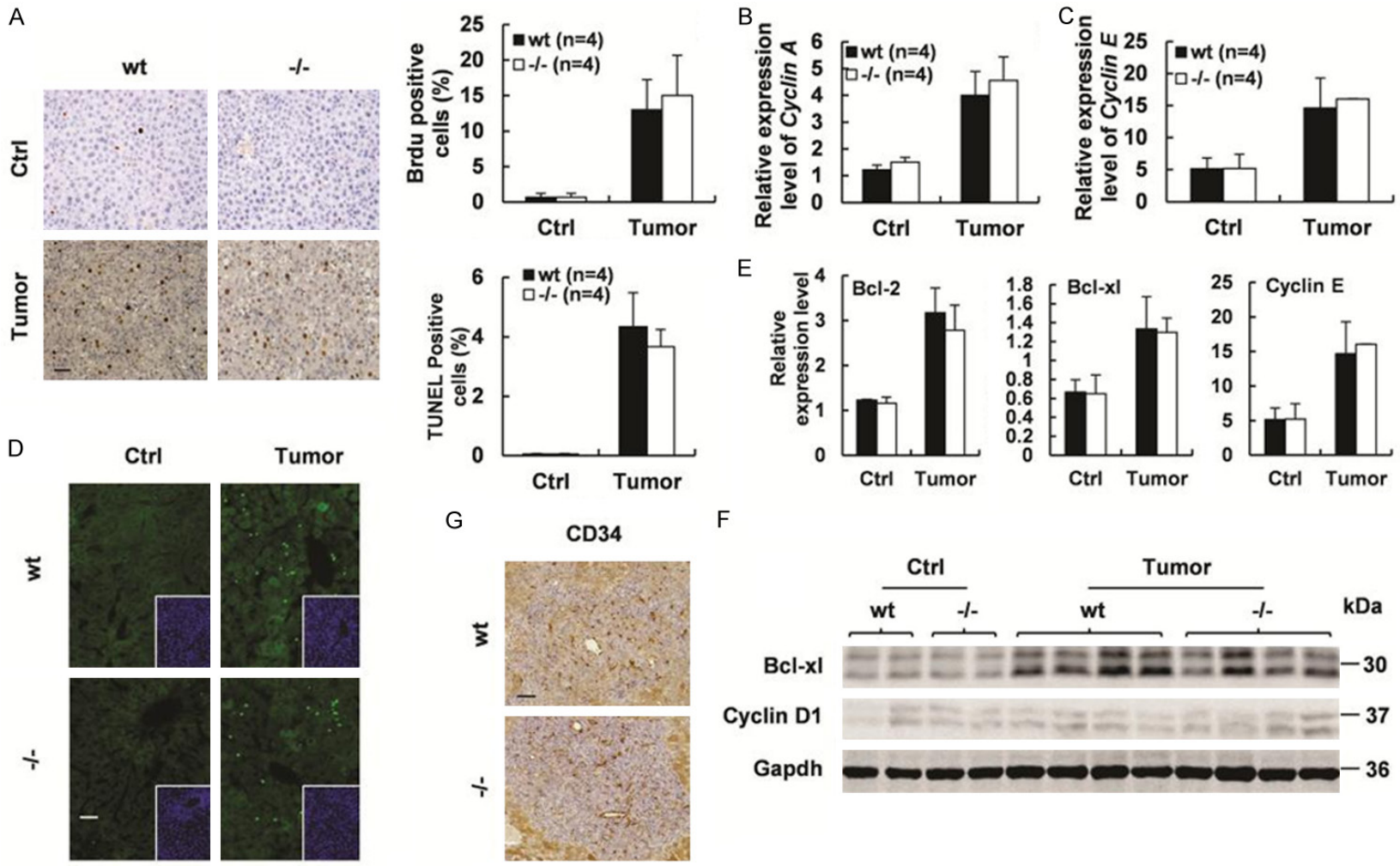

Supplementary Figure 9. Gpr110 did not affect proliferation, apoptosis, or vascularization of tumor in vivo. (A) Immunohistochemical of BrdU in tumor area about liver sections from *Gpr110*$^{-/-}$ mice and wild-type littermates injected with DEN plus CCl_4 after 5 month, quantified by statistical analyzing percentage of positive cells in 20 high-power fields. Scale bar, 50 μm. Values are presented as mean ± SD. **p*<0.05; ***p*<0.01. (B, C) qRT-PCR analyses for *Cyclin A* and *Cyclin E* mRNA expression in liver tumors from (a). Values are presented as mean ± SD from three independent experiments. **p*<0.05; ***p*<0.01. (D) TUNEL staining of liver sections from (A), quantified by statistical analyzing percentage of positive cells in 20 high-power fields. Scale bar, 50 μm. Values are presented as mean ± SD. **p*<0.05; ***p*<0.01. (E) qRT-PCR analyses for *Bcl-2, Bcl-xl,* and *Cyclin E* mRNA expression in liver tumors from (A). Values are presented as mean ± SD from three independent experiments. **p*<0.05; ***p*<0.01. (F) Western blot analysis of Bcl-xl and Cyclin D1 in 5 month CCl_4-treated *Gpr110*$^{-/-}$ mice and wild-type littermate mice liver. (G) Immunostaining of CD34 in the liver sections from (A) (200x). Scale bar, 50 μm.

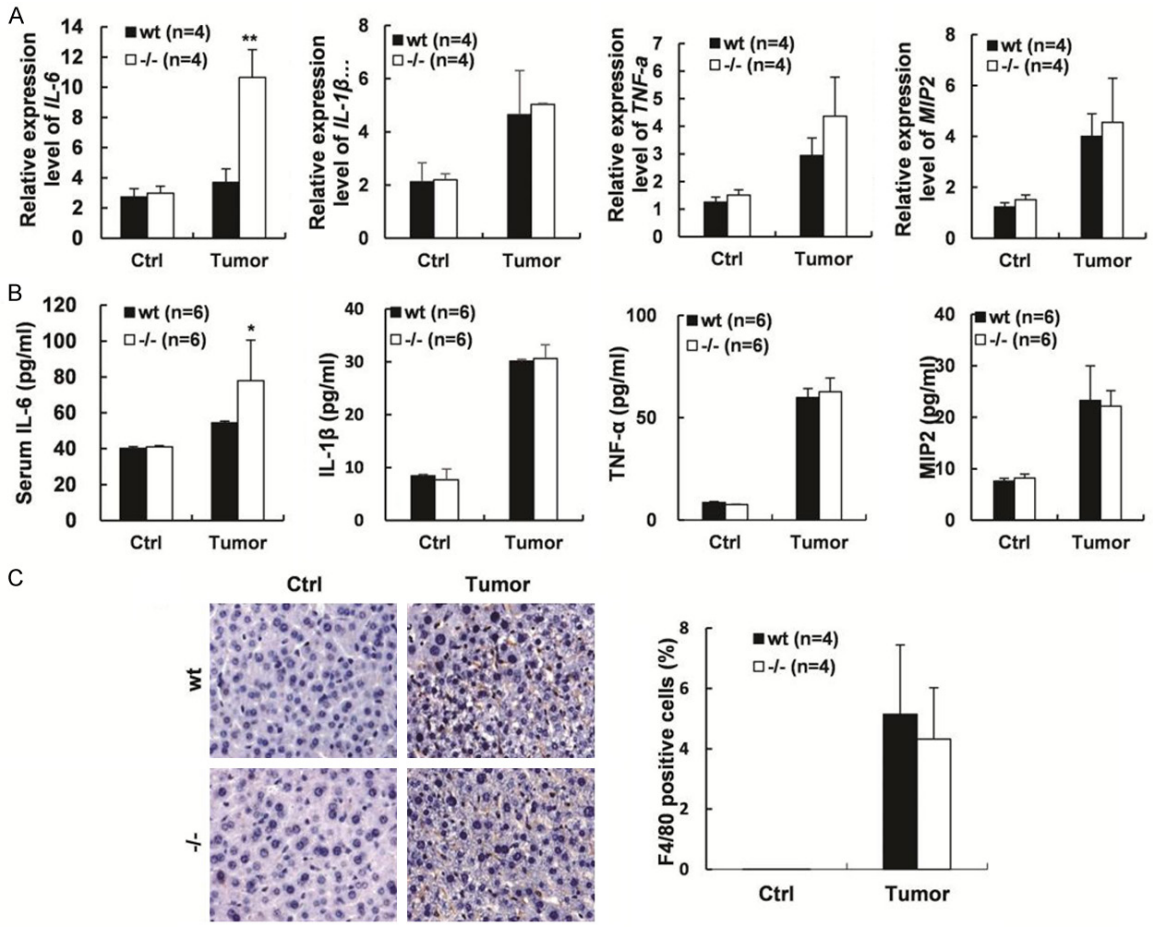

Supplementary Figure 10. Gpr110 did not affect inflammation of tumor induced by CCl_4. A. qRT-PCR analyses for *IL-6*, *IL-1β*, *TNF-α* and *MIP2* mRNA expression in wild-type and *Gpr110*$^{-/-}$ mice liver tumors treated with CCl_4 for 5month (n=4). Values are presented as mean ± SD. **p*<0.05; ***p*<0.01. B. ELISA analysis of serum levels of IL-6, IL-1β, TNF-α and MIP2 in wild-type and *Gpr110*$^{-/-}$ mice liver tumors treated with CCl_4 for 5 month (n=4). Values are presented as mean ± SD. **p*<0.05; ***p*<0.01. C. Immunohistochemical staining of F4/80, sections from *Gpr110*$^{-/-}$ mice and wild-type littermate liver tumors after the CCl_4 injection for 5 month (200×), quantified by statistical analyzing percentage of F4/80 positive cells in 20 high-power fields. Values are presented as mean ± SD. **p*<0.05; ***p*<0.01.

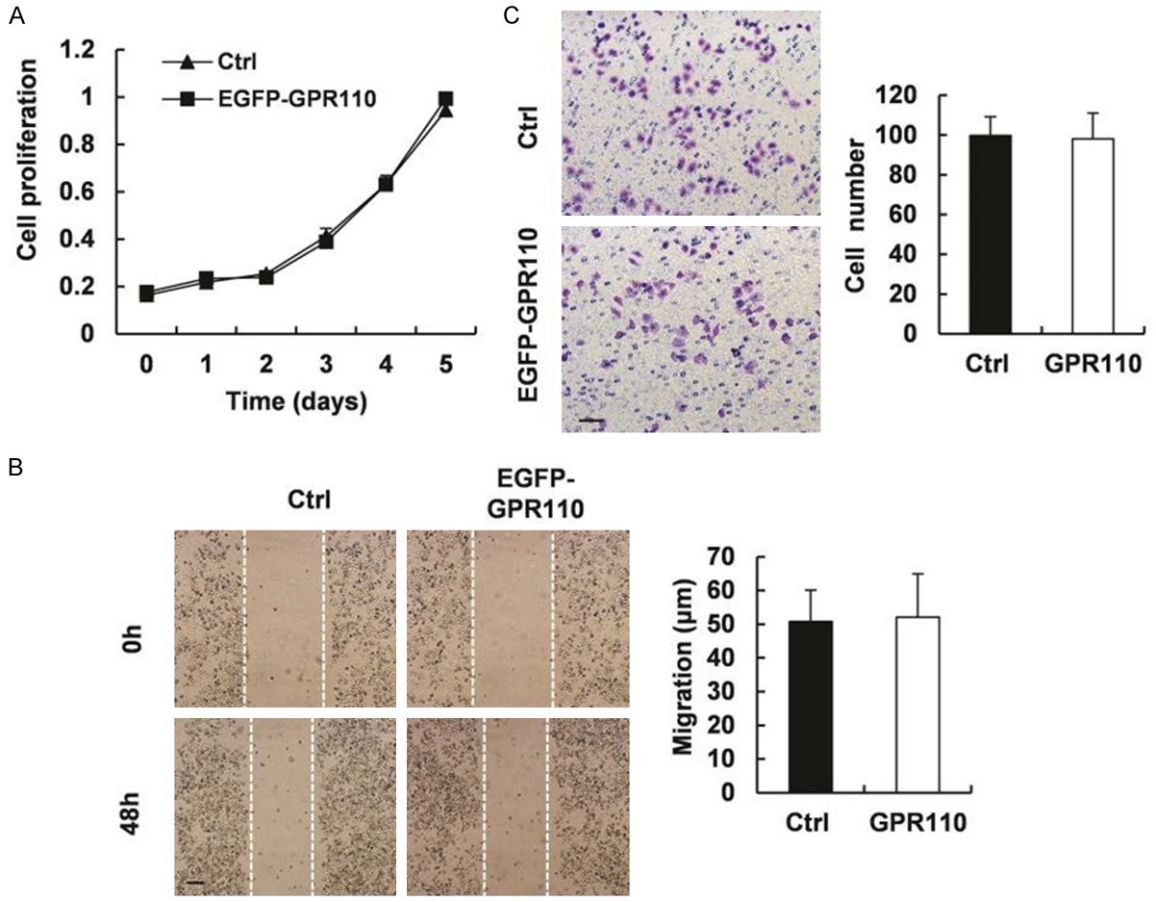

Supplementary Figure 11. Gpr110 had no effect on cell biology function in vitro. A. Cell Counting Kit tested cell proliferation curve in Huh-7 cells after instantaneous overexpression of GPR110. B. Wound-healing assay analysis cell migration ability; migration distance was measured and statistical analyzed. Scale bar, 200 μm. Data shown are means (± SD) from three independent experiments. C. Transwell assay analysis cell migration ability; the cell number was counted and statistical analyzed. Scale bar, 100 μm. Data shown are means (± SD) from three independent experiments.

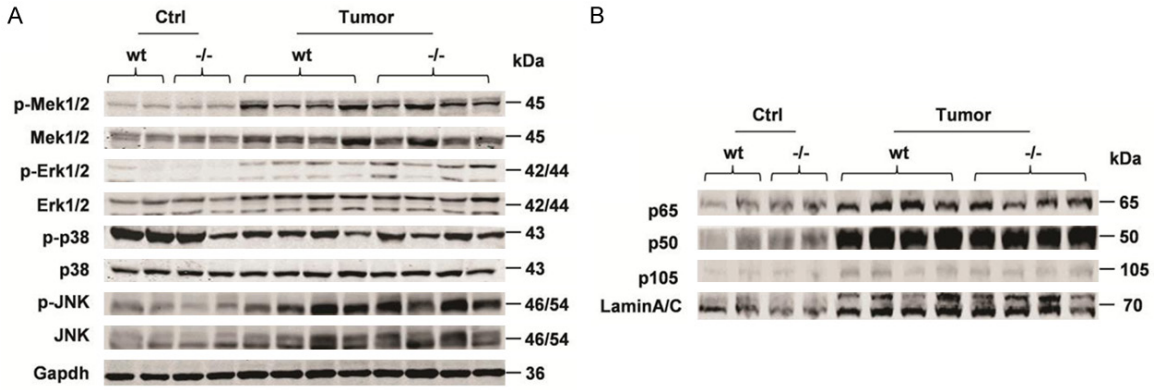

Supplementary Figure 12. Deletion of *Gpr110* did not influence ERK, NF-kB, JNK, or p38/MAPK activation. A. Immunoblot staining analysis of p-Mek1/2, Mek1/2, p-Erk1/2, Erk1/2, p-p38, p38, p-JNK, JNK, in olive oil and DEN plus CCl_4-treated 5 month *Gpr110*$^{-/-}$ mice and wild-type littermate mice liver (n=6). B. Immunoblot staining analysis of nuclear levels of p65, p50, and p105 in olive oil and DEN plus CCl_4-treated 5 month *Gpr110*$^{-/-}$ mice and wild-type littermate mice liver (n=6).